Titre: Title:	Determination of Galloping for Non-Circular Cross-Section Cylinders
Auteur: Author:	Maryam Zabarjad Shiraz
Date:	2014
Type:	Mémoire ou thèse / Dissertation or Thesis
Référence: Citation:	Zabarjad Shiraz, M. (2014). Determination of Galloping for Non-Circular Cross-Section Cylinders [Mémoire de maîtrise, École Polytechnique de Montréal]. PolyPublie. https://publications.polymtl.ca/1404/

UNIVERSITÉ DE MONTRÉAL

DETERMINATION OF GALLOPING FOR NON-CIRCULAR CROSS-SECTION CYLINDERS

MARYAM ZABARJAD SHIRAZ
DÉPARTEMENT DE GÉNIE MÉCANIQUE
ÉCOLE POLYTECHNIQUE DE MONTRÉAL

MÉMOIRE PRÉSENTÉ EN VUE DE L'OBTENTION
DU DIPLÔME DE MAÎTRISE ÈS SCIENCES APPLIQUÉES
(GÉNIE MÉCANIQUE)
AVRIL 2014

UNIVERSITÉ DE MONTRÉAL

ÉCOLE POLYTECHNIQUE DE MONTRÉAL

Ce mémoire intitulé :

DETERMINATION OF GALLOPING FOR NON-CIRCULAR CROSS-SECTION CYLINDERS

présenté par : ZABARJAD SHIRAZ, Maryam
en vue de l'obtention du diplôme de : Maîtrise ès sciences appliquées
a été dûment accepté par le jury d'examen constitué de :

M. GARON André, Ph.D., président
M. PELLETIER Dominique, Ph.D., membre et directeur de recherche
M. ETIENNE Stéphane, Doct., membre et codirecteur de recherche
M. HAY Alexander, Ph.D., membre et codirecteur de recherche
M. CAMARERO Ricardo, Ph.D., membre

DEDICATION

To all who taught me freedom

ACKNOWLEDGEMENTS

First and foremost I express my sincerest gratitude to my supervisor Professor Dominique Pelletier for his support and the confidence he put in me during these years.
I am also extremely grateful to my codirector Professor Stéphane Etienne for his guidance and patience during this research.
I would like to acknowledge my other codicector Doctor Alexander Hay for his guidance and help.
I wish to thank Professors Camarero and Garon, for their time and attention in making constructive criticisms of my thesis.
I cannot find the words to thank my parents for their support and patience. I owe my deepest gratitude to Mehdi for his unflagging love that means everything for me.
I would like to thank my friends and all who supported and taught me during my life.

RÉSUMÉ

Le galop en translation et en torsion d'en cylindres différentes de sections à de faible valeurs du nombre de Reynolds est étudié par le biais de simulations bidimensionnelles. Une formulation par éléments finis spécialement conçue pour les interactions fluide-structure été utilisée. Les équations de Navier-Stokes pour un écoulement de fluide incompressible et les équations du mouvement de le structure sont résolues de maniére fortement couplé. La performance d'un critère quasi-stationnaire visant à prédire le galop est également évaluée sur la base de simulations autour de cylindres fixes pour différents angles d'attaque. L'amortissement et l'inertie induits par l'écoulement sont calculée à partir d'oscillations forcées en rotation. Enfin, la réponse angulaire libre de cylindres rigides montés sur ressorts en torsion est obtenue à partir de simulations d'interaction fluide-structure. Les résultats pour le galop en translation montrent que les prédictions obtenu àes partir du critère quasi-stationnaire sont en très bon accord avec les résultats d'interactions fluide-structure directs. Les résultats en de torsion montrent par contre que le modéle quasi-stationnaire surprédit les zones d'instabilités dynamique.

ABSTRACT

The occurrence of translational and torsional galloping for a square cylinder and of a generic bundle are assessed at low Reynolds number through two-dimensional simulations. A finite element formulation specifically designed for fluid-structure interactions has been used. Incompressible Navier-Stokes equations for fluid flow and structural motion equations are solved in a fully coupled manner. A quasi-steady criterion for predicting galloping is also evaluated based on flow simulations around fixed cylinders for various angles of attack. The flow-induced damping and inertia coefficients of torsional galloping are calculated from a forced rotational oscillation model. Finally, the free angular response of rigid cylinders mounted in cross-flow are obtained from fully coupled fluid-structure simulations. Results for the translational motion of a bundle show that the prediction of quasi-steady criterion are in a very good agreement with direct fluid structure interaction results. Results for the torsional case show that fixed and forced rotations of the cylinders are able to predict quite well the static deflection angles and instability ranges respectively.

TABLE OF CONTENTS

LIST OF TABLES

LIST OF FIGURES

CHAPITRE 1

INTRODUCTION

1.1 Background and Motivation

The study of fluid-induced vibrations of a structure is important in many engineering fields such as aeronautical, offshore, civil and mechanical engineering. Two important fluid-induced vibrations which play a critical roles in designing the structures placed in fluid flows, are Vortex-Induced Vibration (VIV) and galloping Fig.(1.1). Both Mechanisms can lead to high oscillation amplitudes which can result in significant damage to the structures.

VIV results from the two unstable separated shear layers which form discrete vortices lead to os-

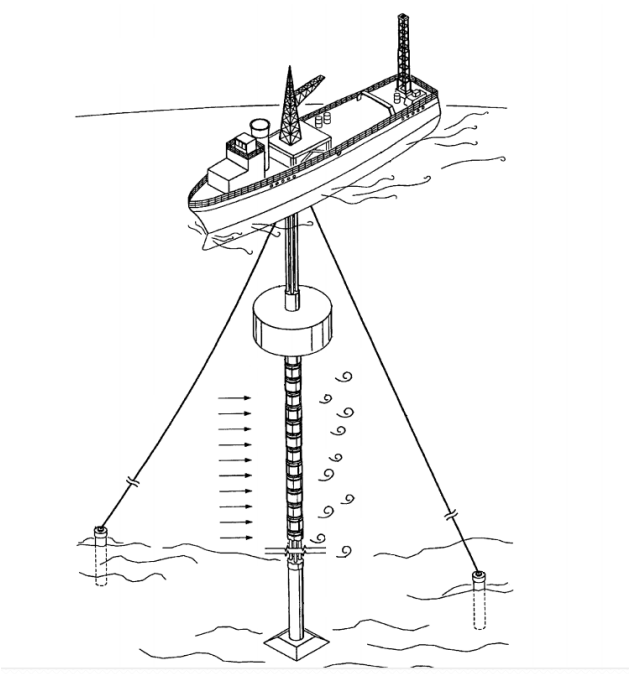

Figure 1.1 Marine structures in the oil industry [1]

.

cillatory pressure loading on the back of the structure. When the vortex shedding frequency is close to the natural frequency of the structure, the resulting vibration are termed VIV.

Galloping is caused by a coupling between the flow-induced forces acting on a structure and the structural vibrations. If the oscillating fluid force tends to increase vibrations, the structure is ae-

rodynamically unstable and very large-amplitude vibration can result. Therefore, galloping is a velocity dependent and damping controlled instability which can introduce high-amplitude and low-frequency oscillations. Wind-induced galloping of buildings, bridges and cables has been reported as well as, ocean-current-induced galloping of marine structures such as box piles, cables and riser towers.

Galloping can cause severe damages to structures. The most famous occurrence was the disastrous oscillation and collapse of the Tacoma Narrows Bridge on 7 November 1940 in 68 Km/h wind Fig.(1.2). As illustrated in the figure, the torsional motion of the bridge was very large. Rotational vibrations reached nearly ± 35 degrees of amplitude which ultimately lead to collapse [2]. After the Tacoma Narrows Bridge collapse, one of the main design criteria for all structures, which are exposed external fluid flow, has required considering the fluid-induced instabilities such as galloping.

For transverse galloping, the transverse oscillation structure and the fluid flow motion cause a variation of the effective angle of attack. Thus, the oscillation of the structure changes the angle of attack and causes variation of the aerodynamic forces acting on the structure. Therefore, the variation of flow-induced forces causes variation in the response of the structure. The galloping instability depends on different factors, such as the shape of the structure, the Reynolds number and the angle of attack. Hence, investigating galloping is difficult particularly in the case of torsional galloping. Quasi-steady models work well at predicting transverse galloping but are not appropriate for torsional galloping.

1.2 Outline of Thesis

The goal of this research is the determination of the flow-induced coefficients and stability map of transverse and torsional galloping phenomenon by using the finite element method. In this work, we will investigate the validity of quasi-steady criterion for the transverse and torsional galloping of different geometrical sections of a oscillating structure.

1.3 Thesis organization

This thesis is structured in five chapters, starting with details that led to the motivation of the study and the goals in chapter 1. Chapter 2 presents the background of the galloping modeling and the literature review, along with descriptions of the theories which support investigation of the research areas. In chapter 3, the translational galloping of structure with quasi-steady criterion and direct fluid structure interaction are investigated. Chapter 4 presents the torsional galloping model. We will discuss results from the quasi-steady, forced oscillation and direct fluid-structure interaction simulations. The thesis ends by stating the outcomes of this study in chapter 5 and

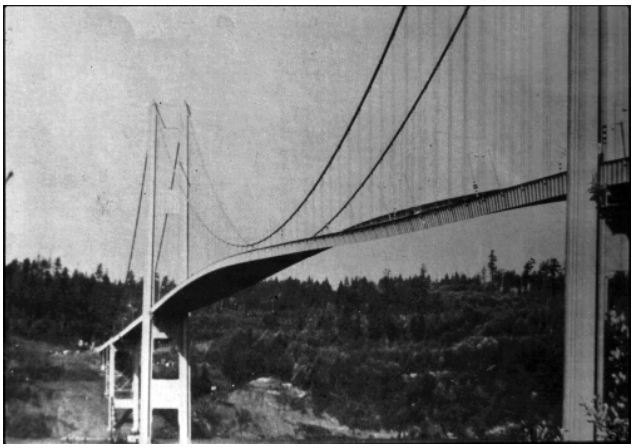

(a)

(b)

Figure 1.2 Figures of the galloping Tacoma Narrows bridge a) before collapse b) after collapse.

proposition for further research possibilities.

CHAPITRE 2

MATHEMATICAL MODELING OF GALLOPING

In the absence of any external forces, the oscillations of a structure decay with time because of the inherent damping which dissipates the oscillation energy. When the structure is exposed to an external fluid flow, aerodynamic forces arise and influence the dynamics of oscillations. In the study of the interaction between flows and structures, the influence of the motion of structures on flow-induced forces has to be considered. Galloping is the instability caused by the variation of aerodynamic forces. Because of the high non-linearity of the galloping phenomenon, and particularly rotational galloping, the simulation of such complicated instability is resource demanding. Thus, we are interested in simulating it by a numerical method which provides for investigation of many parameters effecting galloping with reasonable simulation cost.
This chapter presents a literature review the existing simulation techniques to deal with galloping phenomenon and also numerical approaches to solve obtained models.

2.1 Mathematical modeling

Den Hartog (1956) introduced a very simple criterion for predicting the occurrence of transverse galloping based on the quasi-steady theory which is an approximation to the analysis of the galloping problems [3]. The aerodynamic forces acting on the structure are assumed to be computed by considering the instantaneous relative velocity. This theory assumes that the fluid forces are those acting on a stationary model placed at various angles and it is a quasi-steady model [4].

2.1.1 Translational galloping

The simplest possible explanation of the galloping mechanism is based on the Den Hartog assumption. Fig.(2.1) shows a body in a steady flow of velocity V. In this model, the body is assumed to have only translation motion transverse to the flow. The vertical direction y is defined positive downwards and the body velocity is $u = \dot{y}$. Hence, the angle of attack of the flow relative to the motion model is :

$$\alpha = \tan^{-1}(\dot{y}/V) \tag{2.1}$$

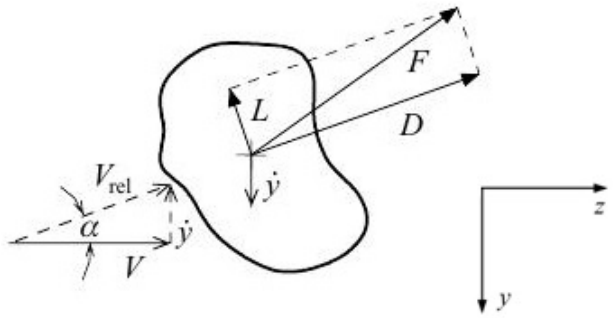

Figure 2.1 one degree-of-freedom galloping model

The lift and drag forces F_L, F_D are in the directions illustrated in figure (2.1). Thus, the fluid force in the vertical direction :

$$F_y = -F_L \cos\alpha - F_D \sin\alpha \tag{2.2}$$

The variation of the fluid force with angle of attack $dF_y/d\alpha$ determines the stability conditions of the model. Thus, increasing the body velocity $\Delta\dot{y} > 0$ results in $\Delta\alpha > 0$. If $dF_y/d\alpha < 0$ with $\Delta\alpha > 0$, then $\Delta F_y < 0$ and is directed upwards and opposite to the direction of $\Delta\dot{y}$, thus it reduces the oscillation and the model will be stable. The model is unstable if : $dF_y/d\alpha > 0$.
It means that if the model is unstable, $\Delta\dot{y}$ and ΔF_y point in the same direction.
Using equation (2.2), $dF_y/d\alpha$ becomes :

$$\frac{dF_y}{d\alpha} = \left(F_L - \frac{dF_D}{d\alpha}\right)\sin\alpha + (-\frac{dF_L}{d\alpha} - F_D)\cos\alpha \tag{2.3}$$

For small enough angles of attack α which result from the small enough velocity $\dot{y}$, equation (2.3) can be written as :

$$\frac{dF_y}{d\alpha} = -(\frac{dF_L}{d\alpha} + F_D) \tag{2.4}$$

Thus, the instability criterion based on the Den Hartog theory, is :

$$(\frac{dF_L}{d\alpha} + F_D) < 0 \tag{2.5}$$

The lift and drag forces are respectively defined as :

$$F_L = \frac{1}{2}C_L\rho V^2 Dl, \quad F_D = \frac{1}{2}C_D\rho V^2 Dl \tag{2.6}$$

where C_L, C_D are the lift and drag coefficients respectively, ρ fluid density, D is the dimension of the body and l is the length of body. Similarly, by considering $F_y = \frac{1}{2} C_y \rho V^2 D l$ and substituting in equation (2.3) yields :

$$\frac{\partial C_y}{\partial \alpha} = -\frac{\partial C_L}{\partial \alpha} - C_D > 0 \;\Rightarrow\; \frac{\partial C_L}{\partial \alpha} + C_D < 0 \tag{2.7}$$

To use equation (2.7) for assessing the stability map of a structure, two aspects should be considered. First, obviously C_D and C_L should be known as a function of α. This data can be measured from experiments or from the monitoring of real structures [5–10]. Next, conditions for which the quasi-steady assumption is valid, should be determined. Obviously, the quasi-steady assumption is valid in low-velocity flows, however from an engineering point of view the low-velocity should be quantified. Two different criteria have been introduced for the validity of the quasi-steady assumption by Fung [11] and Blevins [4].

Based on the Fung criteria, any disturbance imposed on the oscillating body at a particular point must be swept downstream far enough in a period of time so that the disturbance has no effect on the flow around the body. If the velocity of disturbance is equal to the free-stream velocity V, after a period of time the disturbance must be at a distance of V/f_n, where f_n is the frequency of the body oscillation. Fung has suggested that this distance should be at least 10 times the body dimension (D), or $V/f_n D \geq 10$, which is called reduced velocity.

Based on the Blevins criteria, the frequency of the fluid force f_s should be larger than the frequency of oscillation body f_n, $f_s \gg f_n$. This criterion is satisfied at high reduced velocity when :

$$\frac{V}{f_n D} > 20, \tag{2.8}$$

This criterion is easily met in many cases which are prone to galloping instabilities [2].

Bearman *et al.* [12] studied the transverse galloping of a square prism with interference of vortex shedding. They concluded that it is safer to use the quasi-steady theory if the reduced velocity is higher that 30 : $V/f_n D > 30$.

Van Oudheusden [13] studied the second prerequisite for quasi-steady validation. They found that it is essential to define a steady situation for oscillation structure so that it is aerodynamically equal with the unsteady situation. This can be satisfied by defining a proper reference frame.

To obtain a very useful non-dimensional critical flow velocity for galloping, the oscillation body is assumed as a spring-supported, damped modeled satisfying the equation of motion :

$$m\ddot{y} + c\dot{y} + ky = F_y = \frac{1}{2} C_y \rho V^2 D \tag{2.9}$$

in which m is the mass per unit length, c and k the damping and stiffness coefficients per unit length. C_y can be expanded in a Taylor series :

$$C_y = C_y|_{\alpha=0} + (\frac{\partial C_y}{\partial \alpha}|_{\alpha=0})\alpha + ... \tag{2.10}$$

By neglecting C_y at equilibrium ($\alpha = 0$), and substituting $\alpha = \dot{y}/V$ in the above relation, equation (2.9) can be rewritten as :

$$m\ddot{y} + \left[c - \frac{1}{2}\rho V D \frac{\partial C_y}{\partial \alpha}\right]\dot{y} + ky = 0, \tag{2.11}$$

By substituting $c/m = 2\xi\omega_n$, $k/m = \omega_n^2$ in equation (2.11), we obtain :

$$\ddot{y} + 2\omega_n\left[\xi - \frac{\rho V D}{4m\omega_n}\frac{\partial C_y}{\partial \alpha}\right]\dot{y} + \omega_n^2 y = 0 \tag{2.12}$$

where ξ is the damping ratio and ω the natural frequency. The term in brackets is the net damping factor. It is the sum of the structural damping and fluid-induced damping. Instability occur if the net damping becomes negative. Thus, the threshold of galloping when the velocity is equal to $V_{crit} = 4m\omega_n\xi/[\rho D(\partial C_y/\partial\alpha)]$ for reduced velocity is :

$$\frac{V_{crit}}{f_n D} = \frac{4}{(\partial C_y/\partial\alpha)}\frac{m(2\pi\xi)}{\rho D^2} \tag{2.13}$$

The linear theory has been used to predict the critical velocity at which galloping occurs. The question arises as to whether this critical velocity also applies to real engineering structures which exhibit nonlinear behavior. In the next section, the effects of non-linearity on the modeling of galloping are discussed.

Nonlinear effects

In this section, we present the analysis and results that have been obtained by considering the nonlinear terms.
By defining the following nondimensional parameters :

$$Y = \frac{y}{D}, \tau = \omega t, U = \frac{V}{\omega D}, n = \frac{\rho D^2}{2m}, \omega^2 = \frac{k}{m}, 2\xi\omega = \frac{c}{m}, \tag{2.14}$$

equation (2.9) can be written in dimensionless form :

$$\ddot{Y} + 2\xi\dot{Y} + Y = nU^2 C_y, \tag{2.15}$$

where the n is a mass related non-dimensional parameter and the derivation of equation (2.15) are taken with respect to $\tau = \omega t$.
For the square-section model shown of Fig. (2.2), Smith [14] obtained the C_y as a function of

α from experimental measurements done in a wind tunnel. Parkinson and Smith [15] achieved a

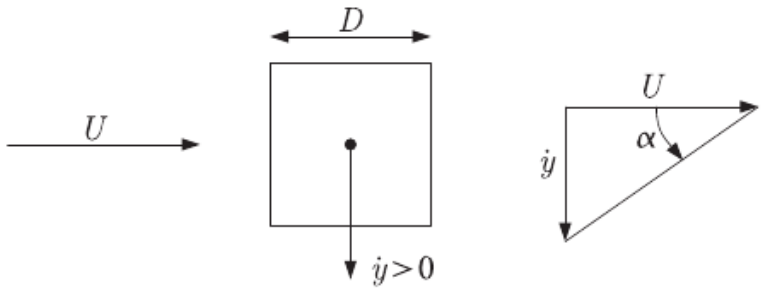

Figure 2.2 A square section model in fluid flow

polynomial approximation based on experimental data :

$$\begin{aligned} C_y &= A\left(\frac{dy/dt}{V}\right) - B\left(\frac{dy/dt}{V}\right)^3 + C\left(\frac{dy/dt}{V}\right)^5 - D\left(\frac{dy/dt}{V}\right)^7 \\ &= A\left(\frac{\dot{Y}}{U}\right) - B\left(\frac{\dot{Y}}{U}\right)^3 + C\left(\frac{\dot{Y}}{U}\right)^5 - D\left(\frac{\dot{Y}}{U}\right)^7 \end{aligned} \tag{2.16}$$

now equation (2.15) yields :

$$\ddot{Y} + Y = nA\left[\left(U - \frac{2\xi}{nA}\right)\dot{Y} - \left(\frac{B}{AU}\right)\dot{Y}^3 + \left(\frac{C}{AU^3}\right)\dot{Y}^5 - \left(\frac{D}{AU^5}\right)\dot{Y}^7\right], \tag{2.17}$$

where the linear damping the first term of the right-hand side of the equation and the other terms of the right-hand side are the higher order velocity dependent terms. However, it is obvious from equation (2.17) that the critical velocity is :

$$U_{cr} = \frac{2\xi}{nA} \tag{2.18}$$

This threshold of galloping is equivalent to the one obtained by linear theory.
The solution for equation (2.17) is not unique and researchers [2, 15, 16] have used different methods to obtain its solutions.

The sectional shape effects

The effects of sectional shape on galloping cannot be neglected because of the effects of body shape on the separation points. Flow separation leads to high pressure on the surface of the body. Thus, the separated flow results in a negative slope of the lift coefficient ($\partial C_L/\partial\alpha < 0$) [17].

However, if there is no afterbody (a part of body in downstream of flow where separation points are), galloping cannot occur [2]. Therefore, in most important shape factor for the galloping is the size of the body (d) relative to its height (h) (d/h). Many researchers [18–21] have investigated the effects of the shape ratio on galloping. Based on these investigations, (d/h) must be large enough for galloping to occur, but not too large to have flow re-attachment on the surface of the structure see Fig.(2.3). Tamura and Itoh [22] numerically studied the effect of shape ratio on the

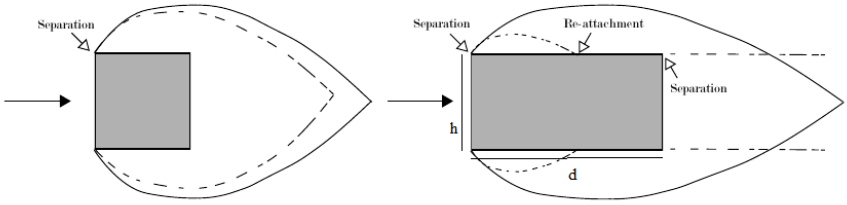

(a) Square cylinder (b) Rectangular cylinder

Figure 2.3 Flow separation on bodies : smooth flow (-), turbulent flow (−−) [17]

transverse motion. The critical depth ratio from their work is smaller than the experimental values. Most studies have investigated the effects of aspect ratio on the translational galloping. Thus, the studying of effects of aspect ratio on torsional galloping is an open research area.

2.1.2 Torsional galloping

If the section of the oscillating structure undergoes a rotational motion because of the flow induced forces (see Fig. 1.2) galloping is labeled as torsional galloping. Most galloping phenomena occurring in the real world and experimental investigations can be termed torsional galloping.
The analysis of torsional galloping is more challenging than that of the transverse galloping because the *(i)* aerodynamic forces depend on both instantaneous angle of attack and angular velocity, and *(ii)* also because the relative flow velocity varies along the section and results in a varying angle of attack along the section. While translational galloping can most of the time be adequately defined by a quasi-steady approach, it is not as straightforward an issue for torsional galloping. Another aspect is the fact the phase difference between the aerodynamic forces acting on the structure and the motion of the structure itself varies with the flow velocity which constitutes another problem in the analysis of the torsional galloping. There is no fully satisfactory solutions to deal with these problems and thus modeling of torsional galloping is an open research area.

Linear quasi-steady analysis

The first attempt to analyze torsional galloping have been adapted from the analysis used for translational to torsional galloping. Fig. (2.4) shows a very simple system related to torsional galloping and in this system the hinge point is not at the geometric center.

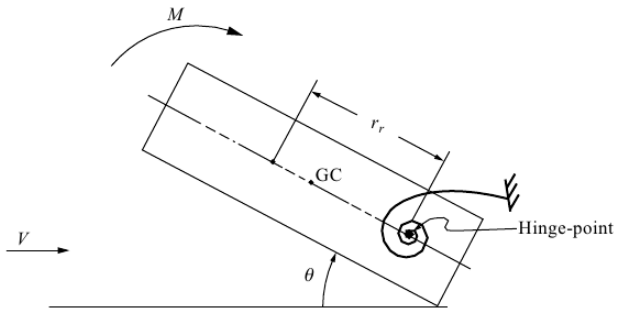

Figure 2.4 Schematic of rectangular section in torsional galloping [2]

In torsional galloping, the angle of attack varies along the section and with the angular velocity. Thus, an approximation is needed for determining the variation of the angle of attack. Therefore, a reference radius r_r on the rotational section is defined such that at an angle γ_r the translational velocity $r_r\dot{\theta}$ is unique and presents the motion of whole section see Fig. (2.5) [2, 4]. A reference

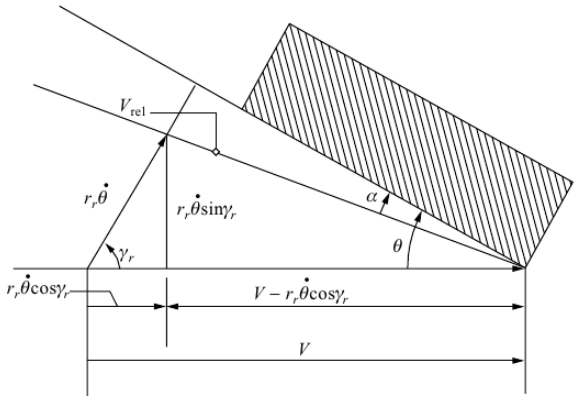

Figure 2.5 Torsional galloping model [2]

angle of attack α, induced by $\dot{\theta}$, and a reference relative velocity are :

$$\alpha = \tan^{-1}\left(\frac{r_r\dot{\theta}\sin\gamma_r}{V - r_r\dot{\theta}\cos\gamma_r}\right) \tag{2.19}$$

$$V_{rel}^2 = \left(r_r\dot{\theta}\sin\gamma_r\right)^2 + \left(V - r_r\dot{\theta}\cos\gamma_r\right)^2 \tag{2.20}$$

For small enough α ($\alpha \ll 1$), equations (2.19) and (2.20) are approximately equivalent with :

$$\alpha \simeq \theta - \frac{r_r\dot{\theta}\sin\gamma_r}{V} \equiv \theta - \frac{R\dot{\theta}}{V} \tag{2.21}$$

$$V_{rel} \simeq V \tag{2.22}$$

where $R = r_r \sin\gamma_r$ is the characteristic radius. Since the definition of r_r is not clear and γ_r depends on θ, equation (2.21) is nonlinear. For a rectangular section rotating about its centroid, Nakamura and Mizota [20] defined R to be half the length of the rectangle. Consequently, α corresponds to the instantaneous angle of attack at the leading edge. Van Oudheusden [13, 23] have considered the simple system shown in the Fig.(2.6). In this model, the depth of the section d is small relative to the distance from hinge point thus that $r_r \approx R$.

The equation governing the torsional motion of the section is :

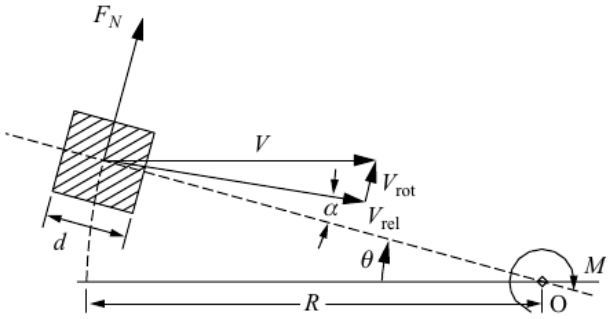

Figure 2.6 Schematic of van Oudheusden model [23]

$$I_\theta\ddot{\theta} + c_\theta\dot{\theta} + k_\theta\theta = M \tag{2.23}$$

where I_θ is the mass moment of inertia of the section, c_θ and k_θ are the torsional damping and stiffness coefficients respectively and M the moment and defined as :

$$M = \frac{1}{2}\rho V^2 h^2 C_M \tag{2.24}$$

where C_M is the moment coefficient and h is a characteristic length. As for the translational case, the C_M can be expanded in a Taylor series :

$$C_M = C_M|_{\alpha=0} + (\frac{\partial C_M}{\partial \alpha}|_{\alpha=0})\alpha + ... \tag{2.25}$$

By neglecting the first term of equation (2.25), and substituting equation (2.21) in the above equation and by defining $C_\theta/I_\theta = 2\xi_\theta\omega_\theta$ and $k_\theta/I_\theta = \omega_\theta^2$, equation (2.25) yields :

$$\ddot{\theta} + \left[2\xi_\theta\omega_\theta + \frac{1}{2}\rho\frac{VRh^2}{I_\theta}\frac{\partial C_M}{\partial \alpha}\right]\dot{\theta} + \left[\omega_\theta^2 - \frac{1}{2}\rho\frac{V^2h^2}{I_\theta}\frac{\partial C_M}{\partial \alpha}\right]\theta = 0 \tag{2.26}$$

This equation has two type of instabilities ; first, the static instability or divergence happens when the stiffness term, sum of the structure and the flow-induced torsional stiffness, goes to zero :

$$\frac{1}{2}\rho V^2 h^2 \frac{\partial C_M}{\partial \alpha} > k_\theta \tag{2.27}$$

The second instability is the torsional galloping which occurs when the damping term becomes negative. The torsional galloping would happen if $\partial C_M/\partial\alpha < 0$. Thus, the critical velocity for threshold of the torsional galloping is :

$$\frac{V_{crit}}{f_\theta h} = -\frac{4I_\theta(2\pi\xi_\theta)}{\rho h^3 R}/\frac{\partial C_M}{\partial \alpha}, \tag{2.28}$$

Investigations [20, 24, 25] on criteria for the threshold of torsional galloping based on equation (2.28) illustrates that it is not reliable. Two drawbacks exist in the theory : "first, approximation the effect of torsional velocity on the angle of attack with a single characteristic point is not viable for complex sections" and second, the torsional motion of the section is sensitive to the vorticity produced by the rotating section while the quasi-steady theory cannot account the related unsteady vortex forces [4, 26]. Therefore, the quasi-steady theory is questionable for torsional galloping and even experimental works which have been done to support using the quasi-steady theory donot agree.

Nonlinear quasi-steady effects

Because torsional galloping is an unsteady phenomenon, the quasi-steady theory approximations for this phenomenon are in poor agreement with experimental data. In the quasi-steady theory the instantaneous moment coefficient, which depends only on the instantaneous position and angular velocity of the structure, is considered and no memory effects is included. Nakamura and his collaborations [20, 27] consider the moment by incorporating the fluid memory effects :

$$M(\theta) = M_\theta \theta + M_{\dot\theta} \dot\theta \tag{2.29}$$

where $M_\theta = \partial M/\partial\theta$ is the "steady aerodynamic torsional moment derivative" and $M_{\dot\theta} = \partial M/\partial\dot\theta$ is the "quasi-steady damping derivative". The $C_\theta e^{-i\phi_\theta}$ and $C_{\dot\theta} e^{-i\phi_{\dot\theta}}$ present the phase correction of quasi-steady responses, thus equation (2.29) yields :

$$M(\theta) = C_\theta e^{-i\phi_\theta} \bar{M}_\theta \theta + C_{\dot\theta} e^{-i\phi_{\dot\theta}} \bar{M}_{\dot\theta} \dot\theta \tag{2.30}$$

where ϕ_θ, $\phi_{\dot\theta}$ are phase delays and overbar variables are quasi-steady values. After substituting and simplifications, the following equation is obtained :

$$-M_{\dot\theta} = -\bar{M}_{\dot\theta} + \lim_{\omega\to 0} (sin\phi_\theta/\omega)\bar{M}_\theta, \tag{2.31}$$

As can be seen in equation (2.31), the stiffness term is now incorporated in the flow-induced damping term. From a physical point of view, equation (2.31) shows that the phase-lag-related damping is associated to the time needed for the viscous flow to adjust to position changes of the structure. The second term of equation (2.31) demonstrates that the unsteady effects can not be neglected. In order to use the quasi-steady theory to analyze torsional galloping properly, the phase delay needs to be considered. However, there is no reliable tool to predict the phase delay. Nakamura and Mizota [20] experimentally measured the $M_{\dot\theta}$ for different aspect ratios. Their results showed that quasi-steady criterion $\partial C_M/\partial\alpha < 0$ for torsional galloping is valid for small aspect ratios (d/h=1,2) but not for higher ratios. Investigations [4, 20, 27, 28] on the quasi-steady theory show that the unsteady fluid dynamics theory is essential to the analysis of torsional galloping. Since, modelling and measurement of unsteady effects in theoretical and experimental investigations are difficult and expensive, numerical analysis a viable alternative for simulation of torsional galloping.

2.2 Multi-degree-of-freedom galloping

Most engineering structures can simultaneously translate and rotate. Galloping has a sporadic nature and is a multi-degree-of-freedom phenomenon in the real world. Thus, the theoretical and experimental works [4, 29–36] have been performed to investigate multidegrees-of-freedom galloping.

Two-degree-of-freedom studies on galloping have been performed by combining the transverse and rotational galloping. Fig.(2.7) shows a simple model which translates vertically and rotates. The springs are fixed to the structure at the elastic axis which does not coincide with the inertial axis. Thus, the equations for the two-degree-of-freedom model shown in Fig.(2.7) are as follows :

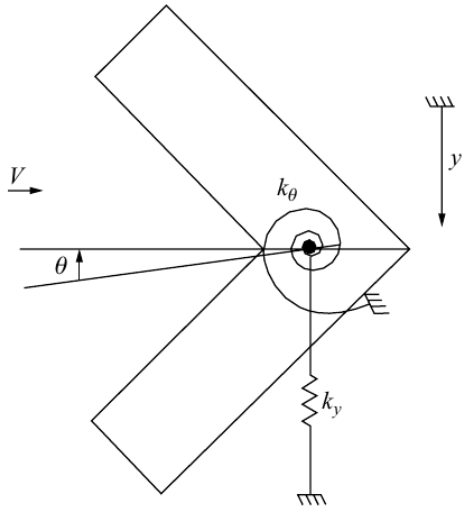

Figure 2.7 A simple two-degree-of-freedom model [4].

$$m\ddot{y} + 2m\xi_y\omega_y\dot{y} + S_x\ddot{\theta} + k_y y = F_y = \frac{1}{2}\rho V^2 D C_y, \tag{2.32}$$

$$I_\theta\ddot{\theta} + 2I_\theta\xi_\theta\omega_\theta\dot{\theta} + S_x\ddot{y} + k_\theta\theta = M = \frac{1}{2}\rho V^2 D C_M, \tag{2.33}$$

where the mass per unit length, mass moment of inertia and the S_x are defined as :

$$m = \int_A \mu d\zeta d\eta, \quad I_\theta = \int_A (\zeta^2+\eta^2)\mu d\zeta d\eta, \quad S_x = \int_A \zeta\mu d\zeta d\eta.$$

where A is the area of the section, μ is the density of the material of the section, ζ and η are coordinates fixed to the section.

The angle of attack according for the quasi-steady theory for small amplitudes is :

$$\alpha = \theta - \frac{r_r \dot{\theta}}{V} + \frac{\dot{y}}{V} \tag{2.34}$$

Based on this model, the two-degree-of-freedom motion is aerodynamically coupled through the angle of attack and S_x. Linear analysis of equations (2.32) and (2.33) yields, the minimum flow velocity for the threshold of galloping as :

$$V = \min \begin{cases} \frac{-4m\xi_y\omega_y - 4b_2^2 I_\theta \xi_\theta \omega_\theta}{\rho D(r_r b_2 + 1)(b_2 D\partial C_M/\partial\alpha - \partial C_y/\partial\alpha)} \\ \frac{-4b_1^2 m\xi_y\omega_y - 4I_\theta \xi_\theta \omega_\theta}{\rho D(r_r + b_1)(-b_1\partial C_y/\partial\alpha + D\partial C_M/\partial\alpha)} \end{cases} \tag{2.35}$$

where $b1$ and $b2$ are defined as :

$$b_1 = \frac{S_x}{m}\frac{\omega_1^2}{\omega_y^2 - \omega_1^2}, \quad b_2 = \frac{S_x}{I_\theta}\frac{\omega_2^2}{\omega_\theta^2 - \omega_1^2},$$

$$\omega_{1,2}^2 = \frac{\omega_y^2 + \omega_\theta^2 \pm (\omega_y^2 + \omega_\theta^2)^2 - 4\omega_y^2\omega_\theta^2(1 - S_x^2/I_{theta}m)^{1/2}}{2(1 - S_x^2/I_\theta m)} \tag{2.36}$$

Equation (2.36) shows that, when the inertia coupling S_x decreases, b_1 and b_2 become close to zero. Thus, equation (2.35) approaches the individual flow velocities for galloping.
Blevins and Iwan [37] have modeled the two-degree-of-freedom motion by considering that the inertial coupling is zero (S_x) from the beginning. They approximated the force and moment coefficients as polynomial functions of α ; $C_y = 0.656\alpha - 7.83\alpha^3$ and $C_M = -0.105\alpha + 9.34\alpha^3$. They found that around the $\omega_\theta/\omega_y \simeq 1$, transverse and torsional motions are strongly coupled otherwise the motion is predominately transverse and the amplitude of motion is in agreement with the individual translational motion.
The poor performance of the quasi-steady theory for the torsional galloping and the need to consider coupling of translational and torsional motion are strong motivation to develop a method for simulating multi-degree-of-freedom in galloping.

2.3 Numerical simulation

Numerical simulations provide a possibility to incorporate more parameters that could influence galloping. Many numerical studies [17, 22, 38–43] have been performed. However only a few of them have investigated torsional galloping.
The governing equations for the motion of a rigid body in a laminar flow are the incompressible

Navier-Stokes equations :

$$\nabla.\mathbf{V} = 0 \tag{2.37}$$

$$\frac{\partial \mathbf{V}}{\partial t} + (\mathbf{V}.\nabla)\mathbf{V} = -\frac{1}{\rho}\nabla P + \upsilon\nabla^2\mathbf{V} \tag{2.38}$$

where $\mathbf{V}$ is the fluid velocity vector, ρ is the fluid density, P is the pressure and υ is the kinematic viscosity of the fluid.

The following equation is used for the motion of a rigid body :

$$\mathbf{M}\ddot{\mathbf{X}} + \mathbf{C}\dot{\mathbf{X}} + \mathbf{K}\mathbf{X} = \mathbf{F} \tag{2.39}$$

where the $\mathbf{M}$, $\mathbf{C}$, $\mathbf{K}$ respectively are the mass, damping and stiffness matrices, and $\mathbf{F}$ is the vector of external forces and moment. Also, $\mathbf{X}$ is the vector of translational displacements in the x and y directions and θ of rotational displacement.

By considering the Navier-Stokes equations for fluid and structural motion equation, we can numerically investigate cases leading to galloping. If the galloping conditions are met, the different parameters in design process can be adjusted to protect against damages caused by galloping.

Tamura and Itoh [22] investigated the critical section of a rectangular cylinder for translational galloping. They used a finite difference method and found that for small aspect ratios flow-induced forces are overestimated compared to the experimental results.

Li *et al.* [39] used a moving frame which is fixed on the rigid body to derive a formulation governing fluid-structure interactions. Then, they applied their formulation to rectangular bodies at $Re = 250$ under forced and free motions which demonstrate the torsional galloping.

Robertson *et al.* [40] used the quasi-steady theory to determine under which conditions rectangular structures undergo translational and torsional galloping. Their results show that the quasi-steady criterion performs well at predicting the threshold of both translational and torsional galloping of rectangular sections.

Joly *et al.* used a 2D finite element method to analyze the translational galloping of square cylinders at low Reynolds numbers. Their model predicts the threshold of translational galloping and its amplitude at high values of mass ratio. However, their quasi-steady model performed poorly at low values of mass ratio.

In this work, we will use a 2D finite element method to analyze the galloping of arbitrary sections. The flow around the structure is considered laminar and incompressible fluid and the solid is treated as a rigid body. A fully coupled formulation using Navier-Stokes equations and the equation of structure is used in this study.

The fundamental basis of almost all CFD problems is the Navier-Stokes equations which are spatial and time dependent. The discretization process is concerned with the transformation of continuous

partial differential equations into discrete equations which are appropriate for numerical computations. In this section, we briefly present the discretization methods for spatial and time.

2.3.1 Spatial discretization

Finite Difference Method (FDM), Finite Volume Method (FVM) and Finite Element Method (FEM) are common spatial discretization methods. Among these numerical methods, the FEM is preferable in this study owing to the ability of the FEM to handle complex geometries and deforming boundaries as well as its flexibility in meshing. Our approach uses the FEM code CADYF that has been developed in the lab of Professor Pelletier.
The FEM is a numerical approach which divides a very complicated domain into small elements. The dependent variable for this system are velocity and pressure for the flow and displacements for the structure. The computational domain is decomposed into N_e elements with N_u nodes for velocity, N_p nodes for pressure and N_x for the displacement. The solution is approximated by using the FEM method for each element as :

$$\begin{aligned} u \approx u_h &= \sum_{i=1}^{N_u} u_i N_i^u \\ p \approx p_h &= \sum_{i=1}^{N_p} p_i N_i^p \\ x \approx x_h &= \sum_{i=1}^{N_x} x_i N_i^x \end{aligned} \tag{2.40}$$

where u_i, p_i and x_i are the velocity, pressure and displacement unknowns at node i and N_i^u, N_i^p and N_i^x are the interpolation functions for the velocity, pressure and displacement respectively.
In the weak form of the Galerkin approach, the test and interpolation functions are the same and there is no equation for the pressure. Several techniques can be used to relate the velocity to the pressure such as the mixed formulation, Uzawa, Penalisation and Augmented Lagrangian Method (ALM). We will use the mixed formulation due to its optimal convergence rate [44].
Discretization is the first step in the procedure of finite element analysis. High accurate results can obtain by utilizing proper discretization techniques and interpolation functions. Discretization can be divided into structured and unstructured techniques. Among them, the unstructured mesh is more appropriate for this study due to its better adaptability for problems with complex geometries.
Several interpolation functions are appropriate for this study such as linear, quadratic which are adaptable for $P_1 - P_1$ and $P_2 - P_1$ elements, respectively. The interpolation function is chosen so that it should satisfy the accuracy level and meet computational cost criteria. The $P_1 - P_1$ element has 3

nodes for velocity and 3 nodes for pressure Fig. (2.8). The velocity and pressure approximations are linear and continuous. However, this element does not satisfy stability condition. The $P_2 - P_1$

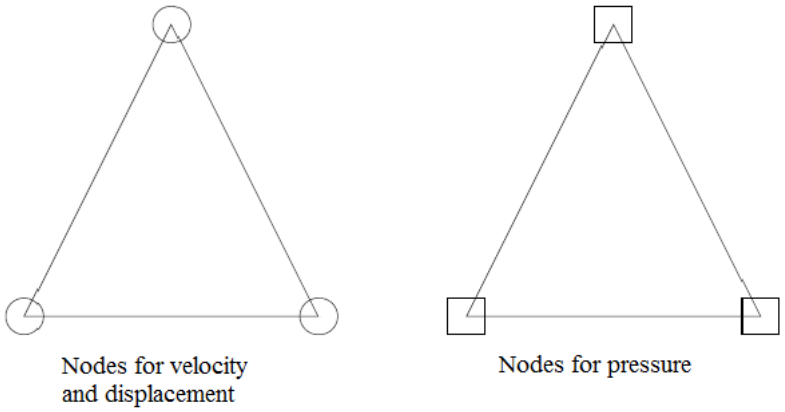

Figure 2.8 $P_1 - P_1$ Element [44]

element has 6 nodes for velocity and 3 nodes for pressure Fig.(2.9). The velocity approximation is quadratic and continuous and pressure approximation is linear and continuous. Hence, the stable Taylor-Hood $P_2 - P_1$ element is used in this study, for the spatial discretization of the velocity u and pressure p.

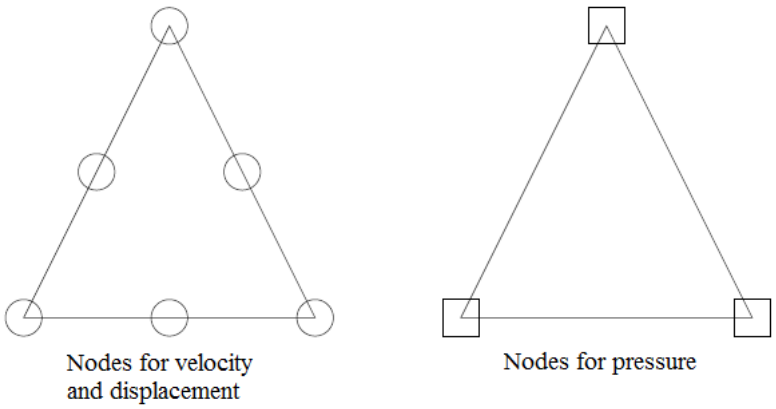

Figure 2.9 Taylor-Hood Element [44]

2.3.2 Time discretization

For many years time integration methods have been intensively investigated for unsteady flow fields which are commonly encountered in engineering applications. Time integration schemes are chosen based on their stability, accuracy and computational cost.
Explicit time integrators are conditionally stable. The time stepsize required for stability is usually much smaller than what is required to get to an acceptable level of accuracy. Explicit schemes are often time consuming for stiff problems [45] while implicit schemes are stable and robust. The time stepsize for implicit schemes is mostly determined based on accuracy considerations and much less restricted by numerical stability requirements. The investigation of phenomena, which may lead to galloping instabilities, needs to use implicit time integrators. Furthermore, the computational efficiency of high-order methods is a strong incentive towards the use of higher order (*i.e.* higher than 2) time integrators. Second-order time integrators are widely used for large scale engineering computations while high-order methods are less often used due to implementation complexity [46].
The one-step multistage Implicit Runge-Kutta (IRK) schemes have been used in flow simulations : Etienne and collaborators [47] have studied Crank-Nicolson, the 1-, 2- and 3-level Radau IIA IRKs for ALE formulation of incompressible flows. Charlot and collaborators [48] have used IRK32 and IRK53 for free-surface flow.
Multistep implicit Backward Difference Formulas (BDF) is another time integration family that is widely used in the computation of large-scale stiff engineering problems [46] because it possesses stiff decay. Although first-order (BDF1) and second-order (BDF2) backwards difference schemes are unconditionally stable, higher-order multistep BDF schemes lose stability for problems for which eigenvalues approach the imaginary axis. Fortunately, the unstable region of the BDF3 is very small. Therefore this scheme can be successfully applied for many unsteady flow computations [49].
Jothiprasad and collaborators have compared a fourth-order IRK64 (1^{st} order for the pressure) with BDF3. They have shown that IRK schemes produce more accuracy with low cost in comparison by BDF. Although, high-order BDF schemes such as BDF3 have high temporal accuracy at modest computational cost, their applications are rather limited due to their tendency to instability for large time step sizes. [49].
Adaptive time integration schemes allow automatic calculation of an optimal time step to adapt the time discretization for following the physics of the flow problem [50]. The Adaptive Trapezoidal Rule (ATR) is a popular adaptive time integration scheme which is used to calculate appropriate time steps in order to avoid oscillations of standard TR. However, ATR scheme can indicate wiggles in some cases. Because of this, Malidi and collaborators [50] have used an Adaptive Backward Differentiation Formula (ABDF) for modeling free surface flows to damp undesired oscillations. In our research group, this idea has been extended to the complete family of BDF schemes. Both step-

size (h-adaptivity) and order (p-adaptivity) selections are performed in a coupled manner. Hence, given a user-chosen error tolerance, the method chooses the order and step-size so that the error tolerance can be satisfied at a low cost.

In this study, we use the adaptive backward differentiation formula with tolerance $10^{-}5$ for time integration.

CHAPITRE 3

TRANSLATIONAL GALLOPING

In this chapter, we analyse the threshold of translational galloping for bundle section cylinders. The quasi-steady theory and direct fluid-structure interaction simulations present the occurrence of translational galloping.
The simulation and analysis of translational galloping for square section cylinder have been performed with our colleagues in Professor Pelletier's lab [42]. We used a finite element based program (CADYF) to perform simulations. Results show that the threshold of translational galloping of a square section is only valid for Reynolds numbers larger than 140. Thus, we consider Reynolds number 200 for the bundle section simulations.

3.1 Bundle

Bundle section cylinders occurs frequently in the design of underwater riser towers or of oil export lines. A bundle is made up of several parallel pipes located in longitudinal grooves of a core section. The pipes protrude from the grooves so that the bundle has a noncircular cross section Fig.(3.1). Thus, the bundle in the flow may exhibit for the galloping instability.
In this work, we consider a bundle section already tested for transverse galloping by Damblans *et*

Figure 3.1 Riser tower bundle [9]

al. [51]. A configuration of the flow around the bundle at zero angle of attack is shown in Fig.(3.2). The Reynolds number is set to 200. The characteristic length D corresponds to the effective diameter of the fictitious circle shown in dotted lines on Fig.(3.3).

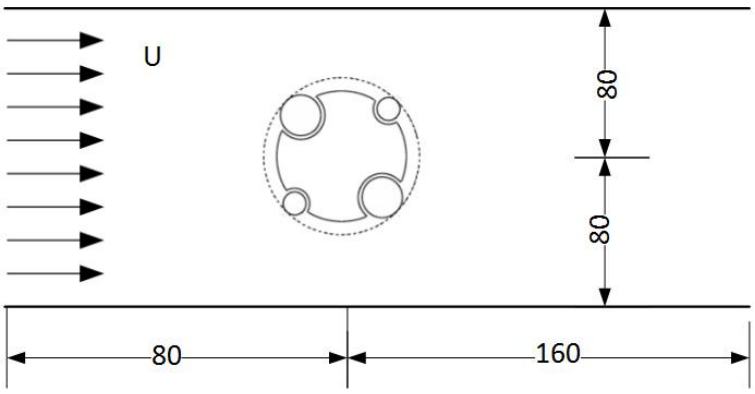

Figure 3.2 Computational domain and fluid flow velocity orientation for the bundle

A convergence study was performed for the flow around a bundle cylinder which includes five

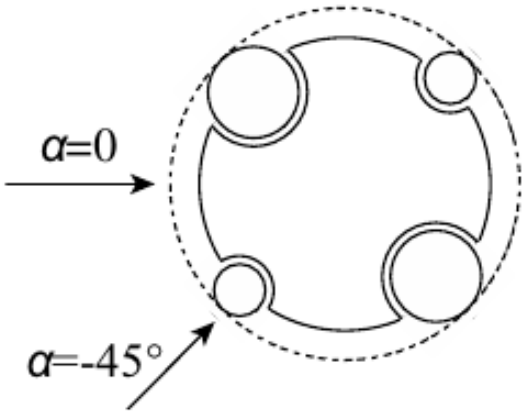

Figure 3.3 Arrangement of the mechanical system : notations and sign orientations

parallel pipes at a Reynolds number of 100. The mesh makes up of $P2-P1$ element has sufficient accuracy. The drag and lift coefficients (C_D and C_L) are shown in Fig.(3.4). As can be seen in Fig (3.4), when the mesh is refined, the results obtained from meshes 40,000, 80,000 and 160,000 are very close. Thus, all numerical computations have been obtained with meshes made of around 50,000 nodes.

The mesh was refined in two areas : in wake area and close to the bundle section. Fig.(3.5) shows a close-up view of the mesh. The mesh density close to the bundle is increased to ensure a good resolution of the flow.

The quasi-steady and direct fluid-structure interaction simulations will been performed using this mesh at different angles of attack. We will rearrange the mesh for different angles of attack so that

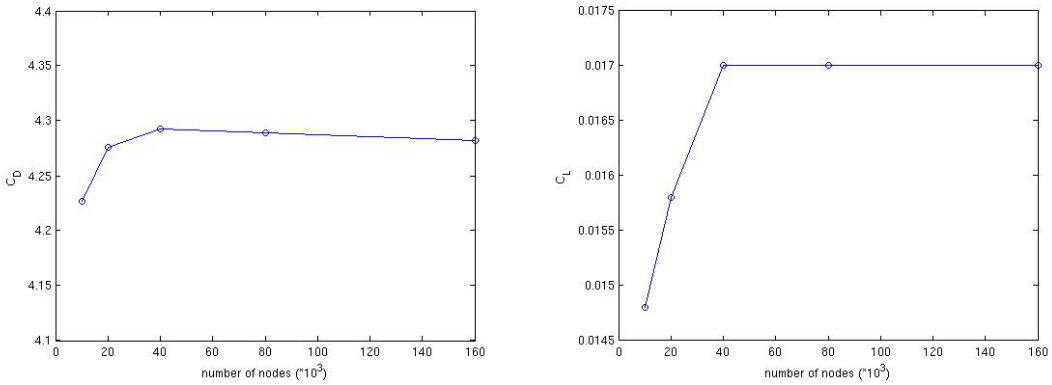

Figure 3.4 Convergence as a function of the number of nodes

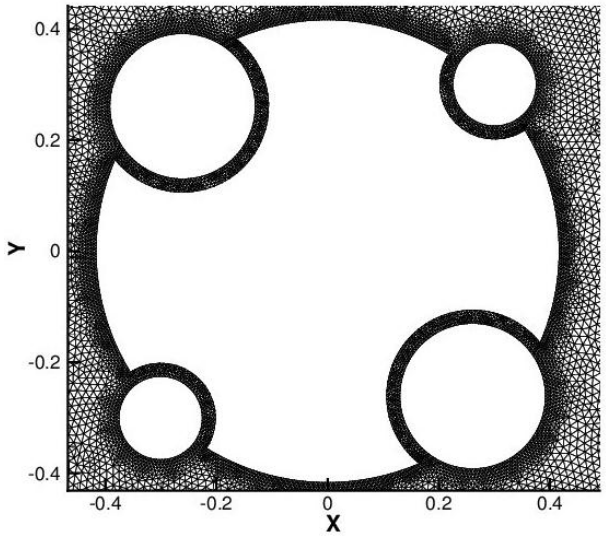

Figure 3.5 Arrangement of the mechanical system : notations and sign orientations

the quality and density of mesh is similar to that for the mesh at zero angle of attack. The following section presents results from the quasi-steady model and from full fluid structure interaction simulations.

3.1.1 Quasi-steady model

In this section a steady simulation has been performed to determine data required for the quasi-steady model prediction of the galloping threshold. The time average values of lift and drag coefficients as functions of the angle of attack are shown in Fig.(3.6) and Fig.(3.7) respectively. As

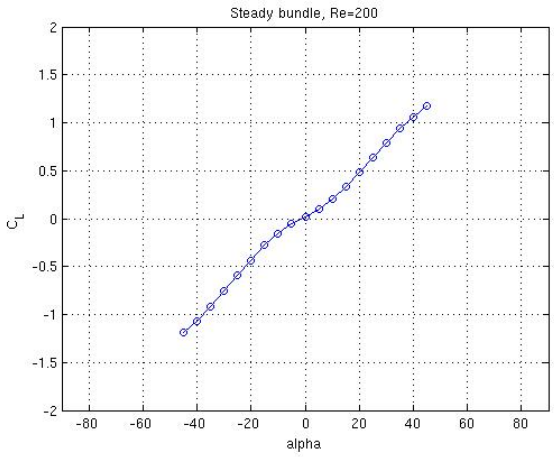

Figure 3.6 The lift coefficient, C_L for the bundle section

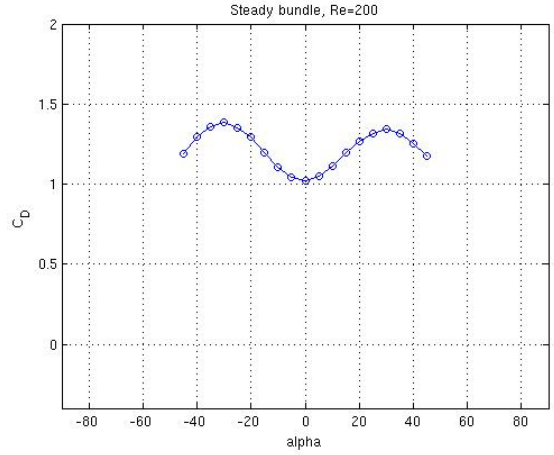

Figure 3.7 The drag coefficient, C_D for the bundle section

can be seen in figures, the quasi-steady criterion ($\partial C_L/\partial\alpha + C_D < 0$) is not satisfied in this case. Thus, the quasi-steady theory predicts no translational galloping for bundle section at a Reynolds number of 200. In the following section, the direct fluid structure interaction simulation has been performed in order to investigate the validating of quasi-steady prediction.

3.1.2 Direct fluid structure interaction

Direct Fluid Structure Interaction (FSI) simulations have been performed in order to analyze the threshold of translational galloping. We investigate the translational galloping for three angles of attack ($-45, 0, 45$ degrees) by FSI. The following equation governs the translational motion of

the bundle :

$$m(\ddot{y}+2\xi\omega\dot{y}+\omega^2 y)=F_y=\frac{1}{2}\rho_{fluid}U^2DC_y \tag{3.1}$$

where m is the mass per length of structure, ξ is the damping ratio, ω is the natural frequency of the structure and C_y is the lift coefficient.
The structural damping has been neglected for all computations and the reduced velocity (U_R) is equal to 25. The mass per length and the stiffness coefficient are given by :

$$m=m*/(\rho_f V_s)=0.846,$$

$$\omega=2\pi f_n=\frac{2\pi U}{DU_R}=\sqrt{K/m}\quad\Rightarrow\quad K=m(\frac{2\pi U}{DU_R})^2, K=0.0534$$

The Navier-stokes equations for the fluid and equation (3.1) for the structure are solved in a coupled manner. Fig.(3.8) shows time histories of translational amplitude for angles of attack of $-45, 0$ and 45 degrees. As can be seen in Fig.(3.8) the amplitudes of translational motion do not increase with time and they achieve an established periodic state. This means that no translational galloping happens for bundle section at $Re=200$. The result confirms the quasi-steady prediction for translational galloping of bundle section.

3.2 Summary

The fixed and free translational motion of cylinder simulations have been performed to investigate of occurrence translational galloping. The quasi-steady criterion predicts no translational galloping and the results from direct FSI validate the quasi-steady predictions. We have also performed simulations of bundle section for $Re=400$ and observed no translational galloping. It means that the inherent damping of the system dissipates the oscillation energy so that no translational galloping instabilities are observed.

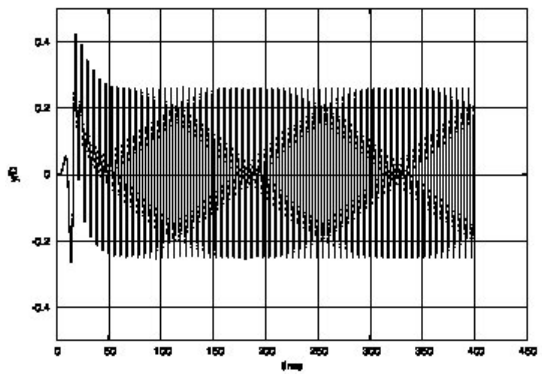

(a) $\alpha = -45$

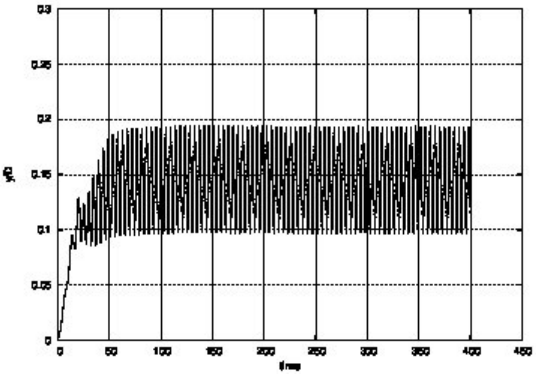

(b) $\alpha = 0$

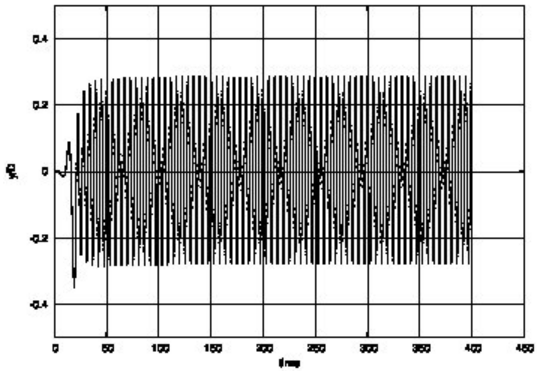

(c) $\alpha = 45$

Figure 3.8 Translational amplitude histories of bundle section

CHAPITRE 4

TORSIONAL GALLOPING

In this chapter, we analyze the threshold of torsional galloping and its amplitude for a square and a generic bundle. Results from the quasi-steady theory, forced oscillation and direct fluid-structure interaction simulations will be presented at low Reynolds number.

4.1 Parameters affecting torsional galloping

The torsional galloping is a very complicated phenomenon which it depends on several parameters. However, dimensional analysis regroups the parameters in 4 key non-dimensional numbers :

— Reynolds number $Re = UD/\upsilon$
where U is the fluid flow velocity, D is the dimension of the section and υ is the kinematic fluid viscosity,

— the reduced velocity $U_R = U/f_n D$
where the $f_n = \omega_n/2\pi$ is the natural frequency of structure,

— the inertia ratio $I^* = I/\rho_f D^4$,

— the structural damping ratio $\xi = c/(2I\omega_n)$.

If we consider the oscillation amplitude A, then the dimensionless amplitude of oscillation will be a function of these parameters :

$$\frac{A}{D} = \Theta(Re, U_R, I^*, \xi) \tag{4.1}$$

Aspect ratio $(D/L)$is another dimensionless parameter which influences the galloping in the varying section of structures, by considering the aspect ratio, equation (4.1) yields :

$$\frac{A}{D} = \Theta(D/L, Re, U_R, I^*, \xi) \tag{4.2}$$

where L is the length of the structure.

The Reynolds number Re in the analysis of torsional galloping for all numerical computations is set to 200 and the reduced velocity U_R is set to 40. The rotational damping is not considered.

All numerical computations are performed using the finite element based program CADYF from the laboratory of Professor Dominque Pelletier. The solver has been specifically designed and developed to treat fluid-structure interactions with rigid or elastic structures. The characteristics of the code for fluid-structure interactions are as follows :

— A fully coupled formulation of the incompressible Navier-Stokes equations with the struc-

tural dynamics equations.

— 3^{rd} order spatial accuracy thanks to the use of $P2-P1$ Taylor-Hood element.

— Up to 5^{th} order time accuracy by using Backward Differencing Formulas (BDF). In this study all simulations have been performed with an adaptive BDF method. The tolerance of the error has been set in time of order 10^{-5}.

— Parallel sparse direct solver PARDISO [52, 53] is used for this work.

— This code has been thoroughly verified for unsteady flows on moving grids [47].

The moment and rotation angles will all be considered positive in the counter-clockwise direction.

4.2 Square section

A two dimensional square is considered in laminar flow at $Re = 200$. A configuration of the flow around a square cylinder at zero angle of attack is shown in Fig.(4.1).

The characteristic length D considered throughout this work corresponds to the edge for the square

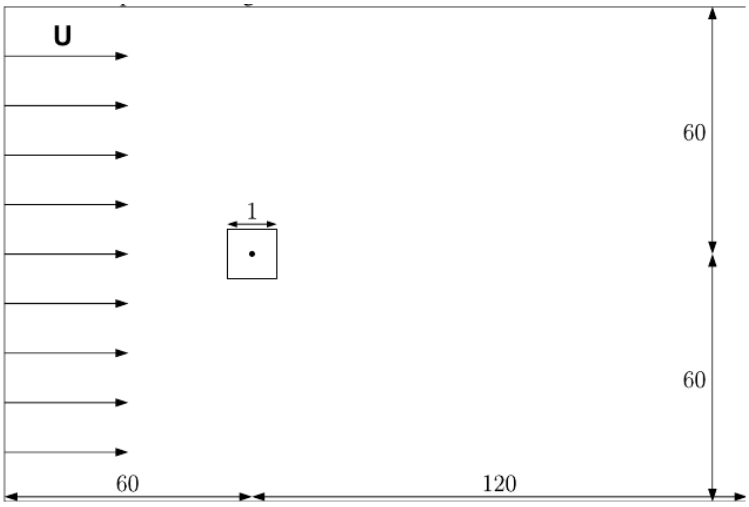

Figure 4.1 Computational domain and orientation of fluid flow velocity.

section as shown in the Fig.(4.2). A convergence study has been performed for the case of the flow around a square cylinder at zero angle of attack at a Reynolds number of 200. This study shows that a mesh of 30,000 nodes is sufficient to ensure 3 digits accuracy on the drag and lift coefficients (C_D and C_L) as shown in Fig.(4.3). As seen in Fig.(4.3), when the mesh is refined, the results obtained from meshes 30,000 and 60,000 are similar. Thus, all numerical computations have been obtained with meshes made of around 50,000 nodes.

Fig. (4.4) and Fig. (4.5) show the mesh employed for the square cylinder simulations. The mesh is refined in the wake and close to the square cylinder. The mesh density close to the walls of the

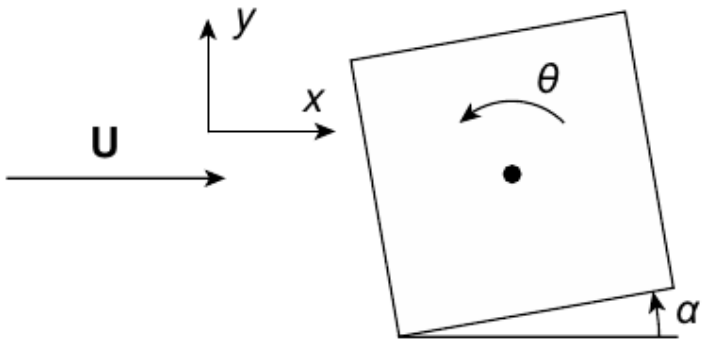

Figure 4.2 Arrangement of the mechanical system : notations and sign orientations

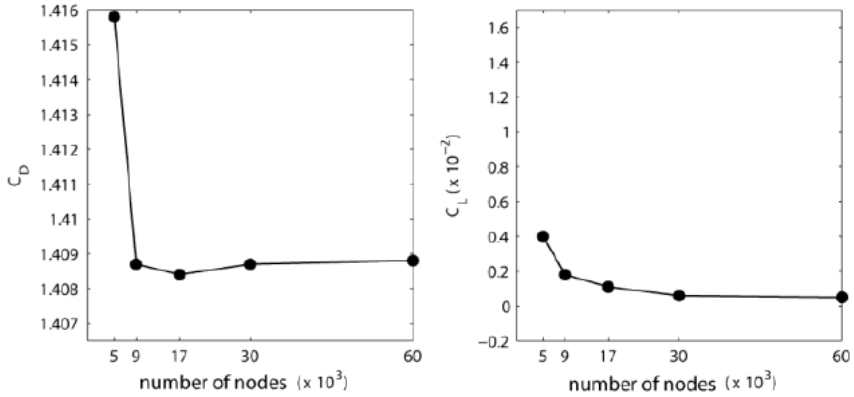

Figure 4.3 Convergence as a function of the number of nodes

square is increased to ensure a good resolution of the flow. The quasi-steady, forced oscillation and direct fluid-structure interaction simulations will be performed by using this mesh at different angles of attack. We will rearrange the mesh for different angles of attack so that the quality and density of mesh are similar to the mesh at zero angle of attack. The next section presents the model and results obtained from each simulations.

4.2.1 Quasi-steady model

The quasi-steady model was very successful at predicting the occurrence and amplitudes of translational galloping [54]. It is natural to begin our study by extending this approach to torsional galloping. This leads to the introduction of a model based on the derivative of the moment coefficient with respect to the angle of attack at different values of the angle of attack.

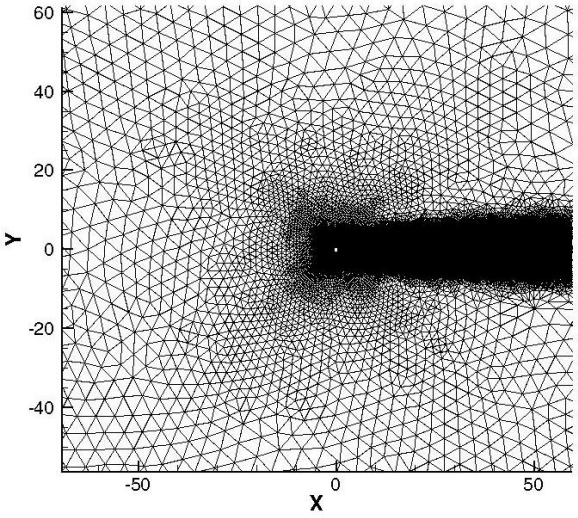

Figure 4.4 General view of the mesh

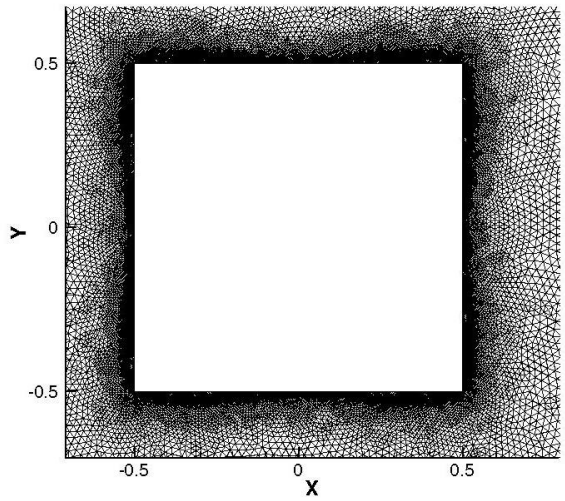

Figure 4.5 Close-up view of the mesh at proximity of the square cylinder.

A steady simulation has been performed to analyze the threshold of torsional galloping by using the quasi-steady criterion. The time averaged value of the moment coefficient as a function of the angle of attack is shown in Fig (4.6). While the square section is symmetric with respect to the flow axis, the moment coefficient is antisymmetric. The C_M values are in good agreement with results obtained by Robertson *et al* [40]. While discrepancies have been observed between the present results and those from the three-dimensional simulation obtained by Yoon *et al.* [43], we suspect that

their results were obtained on too coarse a mesh.

As discussed before, the quasi-steady criterion requires the actual averaged flow induced moment

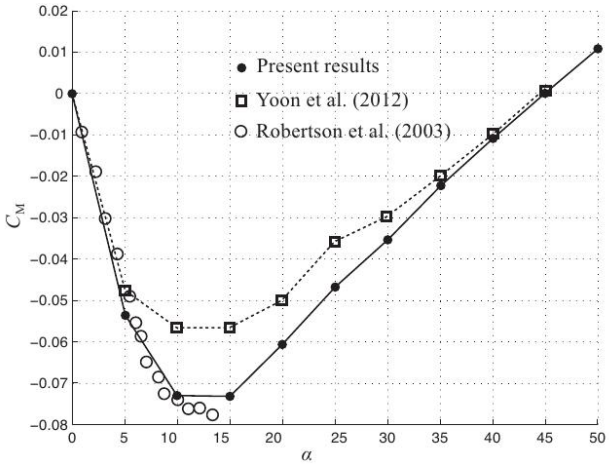

Figure 4.6 C_M for the square section and comparison with Robertson and Yoon results.

at various angles of attack. The galloping criterion is expressed as :

$$-K_\alpha = \frac{\partial M_\alpha}{\partial \alpha} < 0 \tag{4.3}$$

where M_α is the moment ($M_\alpha = 1/2\rho_{fluid}U_\infty^2 D^2 C_M(\alpha)$) and α is the angle of attack. The moment derivative in equation (4.3) can be interpreted as a flow induced linear stiffness term which is denoted as K_α.

As seen in Fig.(4.6), the quasi-steady criterion is satisfied at Angle Of Attack (AOA) ranging from -10 to 10 degrees approximately. In the following, we evaluate the validity of prediction of the instability range from the quasi-steady criterion results. We will first discuss results from forced body rotations in cross-flow and then pursue with the analysis of the direct fluid-structure interaction simulations results.

4.2.2 Forced oscillation

Forced oscillation simulations have been performed to determine the induced fluid flow damping and the added inertia coefficients. The forced rotational oscillation is given by sinusoidal :

$$\theta = \theta_0 sin\omega t \tag{4.4}$$

where the θ_0 is the amplitude of the motion and ω is the angular velocity ($\omega = 2\pi/T$ where $T = 40$ for this study). The fluid flow induced moment can be approximated by :

$$M_\alpha = -K_\alpha \theta - C_\alpha \dot{\theta} - I_\alpha \ddot{\theta} \tag{4.5}$$

Using to equation (4.3), equation (4.5) can be rewritten as :

$$M_\alpha = \frac{1}{2}\rho_{fluid} U_\infty^2 D^2 C_M(\alpha + \theta) - C_\alpha \dot{\theta} - I_\alpha \ddot{\theta} \tag{4.6}$$

Since the stiffness and the inertia have the same phase, we must be able to determine one of the two coefficients to deduce the other one. By multiplying equation (4.6) by $\dot{\theta}$ and taking the average in time, we can determine the damping coefficient by solving equation (4.7) :

$$-C_\alpha \int_t^{t+nT} \dot{\theta}^2 dt = \int_t^{t+nT} M_\alpha(\theta, t)\dot{\theta} dt \tag{4.7}$$

To determine the inertia coefficient, we multiply equation (4.6) by $\ddot{\theta}$ and take the average in time :

$$\int_t^{t+nT} \frac{1}{2}\rho_{fluid} U_\infty^2 D^2 C_M(\alpha + \theta)\ddot{\theta} dt - I_\alpha \int_t^{t+nT} \ddot{\theta}^2 dt = \int_t^{t+nT} M_\alpha(\theta, t)\ddot{\theta} dt \tag{4.8}$$

From the steady simulation, we have been able to determine the averaged moment for the fixed section for several angles of attack. This allowed us to provide a definition for the stiffness term in equation (3.6). We have decided to keep it in the form of the moment without expressing it as the stiffness multiplying to the angle because the moment is a nonlinear function of the angle of attack and it becomes less practical to use a polynomial stiffness function. Thus, it is simpler to keep the values of moments obtained for the steady flows conditions from the previous section for stiffness term. According to our expectation the amplitude of rotational motion is of the order of 20 degrees. Fig.(4.7) shows the fluid flow induced rotational damping for the square section. The values of the coefficients are plotted as a function of forced rotation amplitude for several values of the angle of attack at rest.

As illustrated in Fig.(4.7), the fluid flow damping coefficient is negative up to around 20 degrees for angles of attack at rest of 0 and 5 degrees. Also, the damping coefficient is never negative for an angle of attack of $\alpha = 10$ degree. This indicates that the quasi-steady criterion is too conservative since according to results presented in the steady section, the criterion is satisfied at angles of attack ranging from -10 to 10.

Fig.(4.8) shows the added inertia for the square section. The values of the coefficients are plotted as a function of forced rotation amplitude for several values of the angle of attack at rest.

As seen in Fig.(4.8), the added inertia values are positive except for $\alpha = 0$ degree angle of attack.

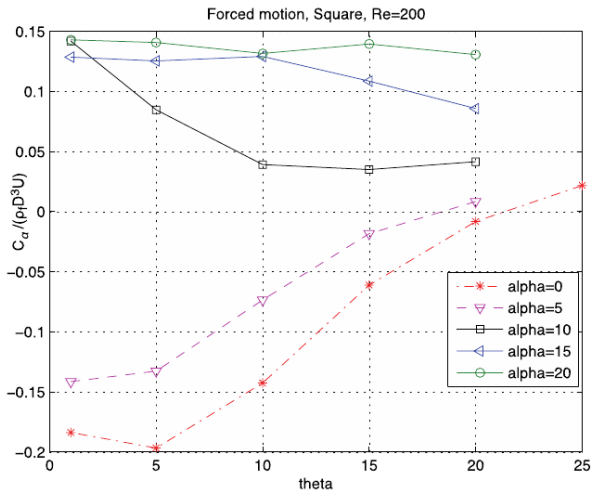

Figure 4.7 Induced fluid flow rotational damping.

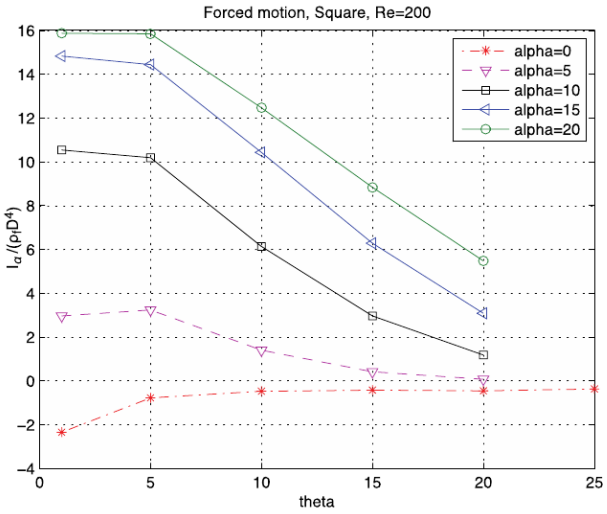

Figure 4.8 Added inertia for the square section

4.2.3 Direct fluid-structure interaction

In this section, we consider the free rotation of square around its central axis. We assume that, the elastic and rotational centers are both located at the centroid of the cylinder. The galloping instability will be determined by solving the following equation governing the free motion of system :

$$I(\ddot{\theta} + 2\xi\omega\dot{\theta} + \omega^2\theta) = M_{fluid} \tag{4.9}$$

where the I is the inertia per unit length of the square, ω the undamped natural frequency of the system, ξ the structural damping ratio and M_{fluid} the fluid moment.
Equation (4.9) and the incompressible Navier-Stokes equations are solved in a fully coupled manner. As mentioned before, the Reynolds number is set to 200 and the reduced velocity is equal to 40. The structural damping has been considered to zero for all simulations. The inertia and stiffness coefficients for the square will be :

$$I = I*/(\rho_f D^4) = 16.67$$

$$f_n = \frac{U}{DU_R}, \omega = 2\pi f_n = \sqrt{K/I} \quad \Rightarrow \quad K = I(\frac{2\pi U}{DU_R})^2, K = 0.411$$

Simulations have been performed for several values of the angle of attack at rest in the range of 0 to 45 degrees in order to compare results with the forced motion case. Fig. (4.9) shows time histories of the rotation angles for several values of the angle of attack. As can be seen in Fig.(4.9), the amplitudes of rotation angle grow when the angle of attack at rest changes from -10 to 10. However, for other angles of attack no of rotation galloping is observed. These results appear to contradict those obtained from forced rotation simulations, but they are in good agreement with the quasi-steady theory predictions.

4.2.4 Summary

The predictions of rotational galloping threshold for square section have been performed based on the quasi-steady criterion, forced rotation and direct FSI simulations Table(4.1). Based on the quasi-steady criterion, rotational galloping occurs at angles of attack at range -10 to 10 degrees. Rotational amplitudes are shown in column 2 and 3 in Table (4.1) for those angles of attack at which galloping occurs. The free rotation results are not in proper agreement with the results of the forced oscillation model. When the section freely rotates, the fluid flow induced stiffness generates a static angular deflection.

For spring mounted cylinders, the average moment induced by the flow generates a change in the apparent angle of attack which is named the effective angle of attack. Columns 5 and 6 in Table (4.1) show the effective angles of attack. To predict the quasi-steady average effective angle of attack the following equation was used :

$$M_\alpha = f(\alpha_{eff}) = K(\alpha_{eff} - \alpha) \tag{4.10}$$

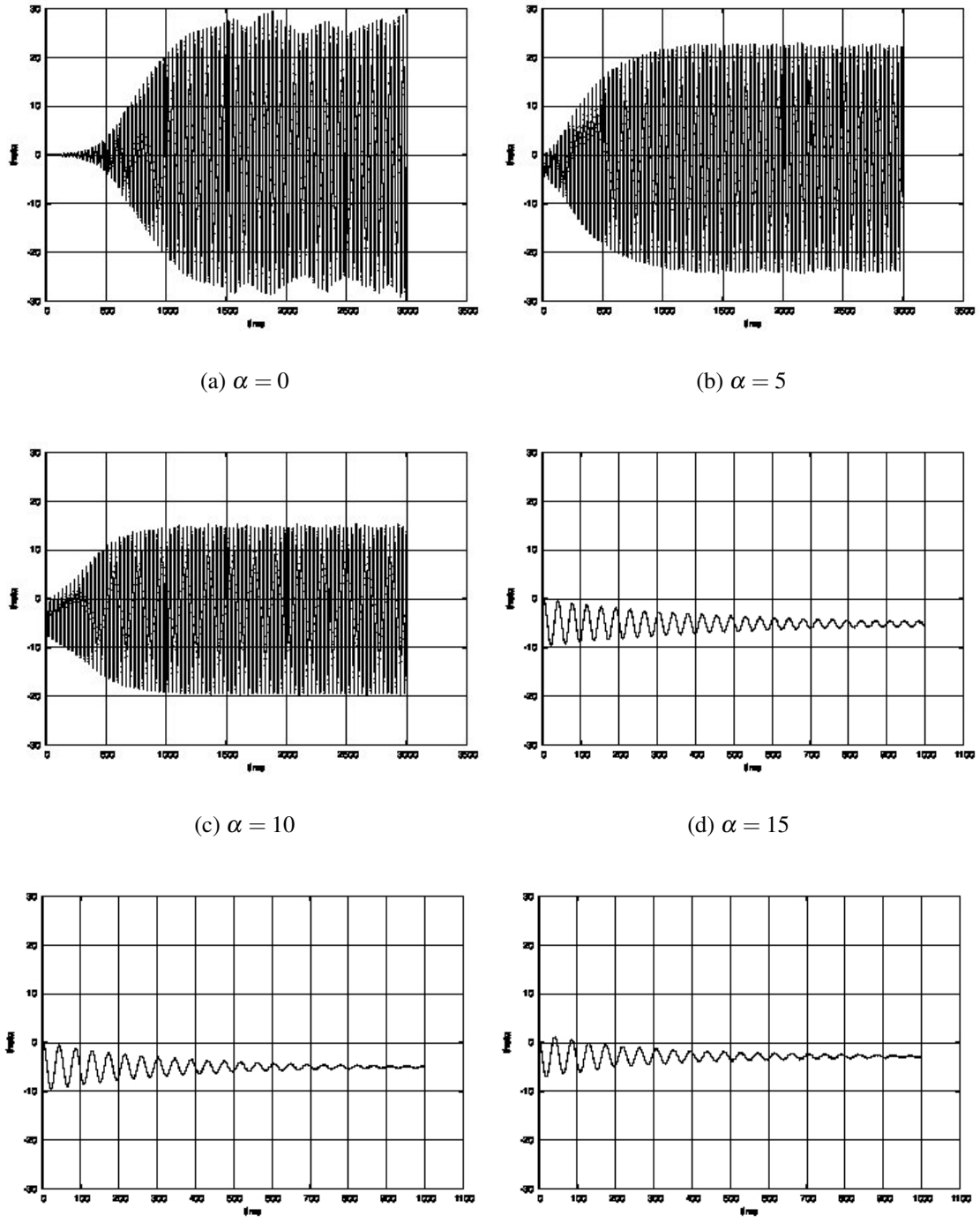

(a) $\alpha = 0$ (b) $\alpha = 5$

(c) $\alpha = 10$ (d) $\alpha = 15$

(e) $\alpha = 20$ (f) $\alpha = 25$

Figure 4.9 Rotation angle histories of square section

This prediction is based on the assumption that dynamic effects have a small influence on the average angle of attack. The effective angle of attack for the FSI simulations was obtained by the

Tableau 4.1 Square cylinder rotational galloping threshold based on the models.

AOA α	**QS**	**Forced θ**	**FSI θ_{max}**	**QS α_{eff}**	**FSI α_{eff}**	**FSI U_R**
0	Yes	22	27	0	0	36.3
5	Yes	18	20	2.9	3	36
10	Yes	No	16	6.0	6.5	35.4
15	No	No	No	9.8	10	37.6
20	No	No	No	15	15	43.3
25	No	No	No			

following equation :

$$\alpha_{eff} = \alpha + \bar{\theta} \tag{4.11}$$

where α is the angle of attack at rest and $\bar{\theta}$ is the time average value of the computed angle of rotation (obtained from Fig.(4.9)).

As seen in Table (4.1), the effective angle of attack is zero when the angle of attack at rest is zero. This is because the section is symmetric with respect to the incoming flow. Also, from the Table (4.1), we can conclude that the quasi-steady and FSI simulations static deflections predictions are generally in agreement.

The observed reduced velocities are given in the last column of Table (4.1). We set a reduced velocity equal to 40, however the observed reduced velocities are lowered by around the 10% for all configurations corresponding to galloping. This is because of the negative flow induced torsional stiffness. The effective added moment of inertia is quite low for the effective rotational amplitudes encountered in direct FSI simulations compared to the solid moment of inertia as can be seen in Fig. (4.8). Thus, it has less effect than the flow-induced stiffness on the observed vibration frequency.

In the next section, the bundle section will be simulated based on the quasi-steady, forced rotation and direct FSI models.

4.3 Bundle section

Bundle section cylinders are most interesting in the design of underwater riser towers or oil export lines. In this work, we consider a bundle section already tested for transverse galloping by Damblans *et al.* [51]. A configuration of the flow around the bundle at zero angle of attack is shown in Fig.(4.10).

We investigate the flow at low velocity the Reynolds number is set to 200 and the characteristic length D considered corresponds to diameter of the fictitious circle in dotted lines on Fig. (4.11).

A convergence study has been performed for the case of the flow around a bundle cylinder which includes five parallel pipes with the Reynolds number set to 100. The drag and lift coefficients (C_D

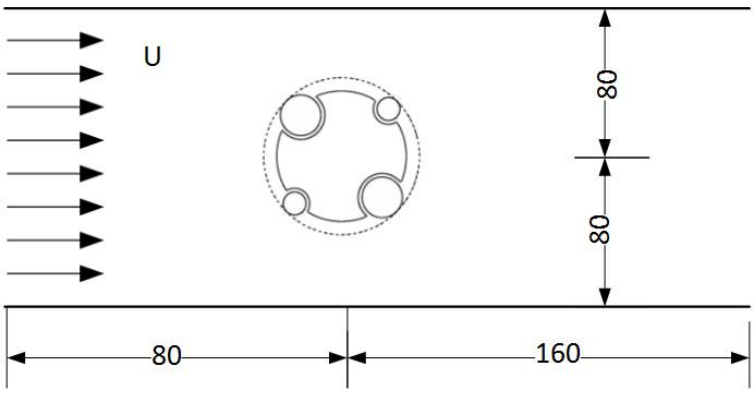

Figure 4.10 Computational domain and fluid flow velocity orientation for the bundle

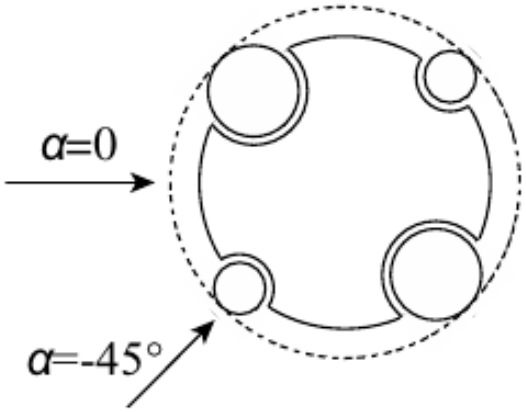

Figure 4.11 Arrangement of the mechanical system : notations and sign orientations

and C_L) as shown in Fig. (4.12). As seen in Fig (4.3), when the mesh is refined, the results obtained from meshes with 40,000, 80,000 and 160,000 nodes are similar. Thus, all numerical computations have been performed with meshes with around 50,000 nodes.

For the bundle section two areas of refinement are considered as for the square section in previous part ; the wake area and the area close to the section. Fig. (4.13) shows a close-up of the mesh. The mesh density close to the bundle is increased to ensure a good resolution of the flow.

The quasi-steady, forced oscillation and direct fluid-structure interaction simulations will been performed with this mesh at different angles of attack. We will rearrange the mesh for different angles of attack so that the quality and density of mesh is similar for the mesh at zero angle of attack. In the following section, the model and results obtained from each of simulations will be presented.

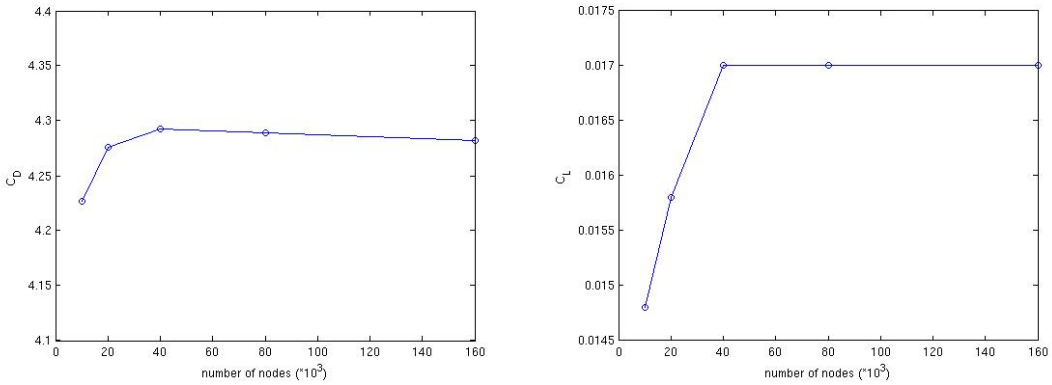

Figure 4.12 Convergence as a function of the number of nodes

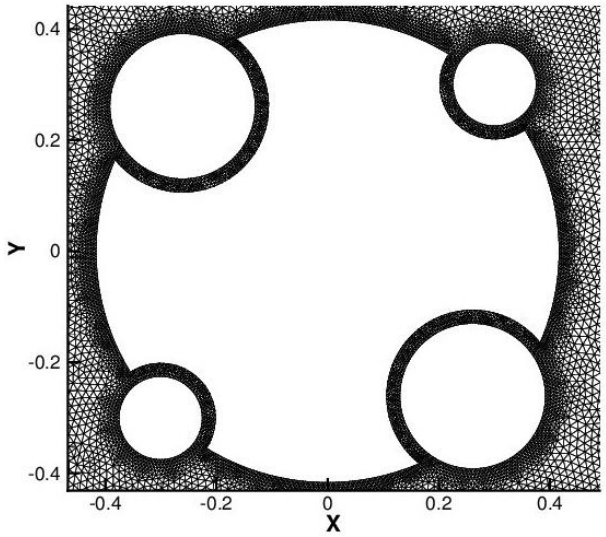

Figure 4.13 Arrangement of the mechanical system : notations and sign orientations

4.3.1 Quasi-steady model

In this section, the quasi-steady criterion is used to predict the threshold of rotational galloping for the bundle. The averaged moment coefficient values as a function of the angle of attack are shown in Fig.(4.14). Following notations of Fig (4.11), there is no symmetry with respect to the midplane. By considering 45 or -45 degrees as a reference, the section would have been symmetric. However, the current choice makes it easier to compare with the square section.

We observe a behavior roughly similar to that of the square section as a function of the angle of

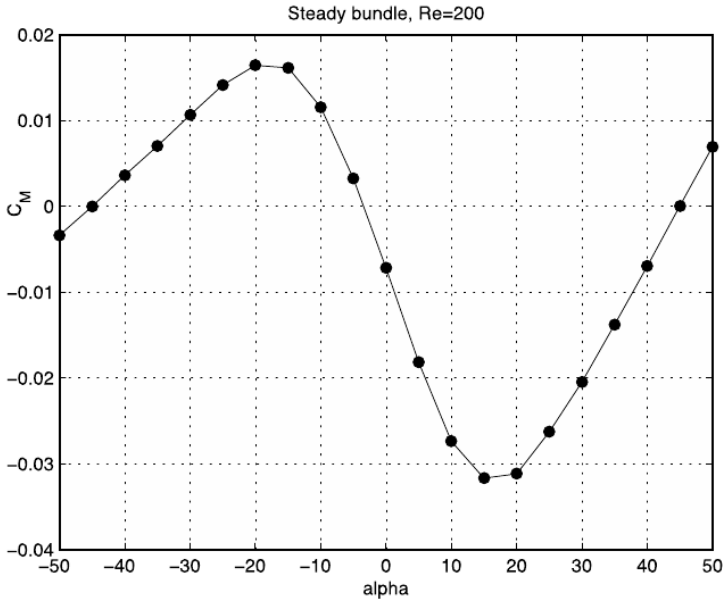

Figure 4.14 Moment coefficient, C_M for the bundle section

attack. However, it is no longer antisymmetric due to the asymmetry of the bundle. The absolute maximum averaged moment is lower than those for the square section. This might be due to two reasons. First recall that the outside diameter is equal to the square section edge. This makes the apparent bundle face smaller than that of the square. And second, the bundle section "corners" are rounded making the cylinder less sensitive to a change in angle of attack.
The quasi-steady criterion for the threshold of the rotational galloping is satisfied for the angles of attack ranging from -10 to 15 degrees approximately. This is similar to the square section. In the following, we will evaluate the quasi-steady criterion for the bundle section. Thus, we will present and discussed the results from the forced body rotations in cross-flow and then end with the analysis of the direct FSI simulations results.

4.3.2 Forced oscillation

Forced rotation simulations are used to determine the induced fluid flow damping and inertia coefficients of the bundle section. As for the square section, a sinusoidal rotation is imposed on the bundle section (see equation 4.4). We have used equations (4.7) and (4.8) to compute the induced fluid flow damping and inertia coefficients, respectively. As discussed before, the stiffness coefficient is defined as a function of the averaged moment from the steady case for several angles of attack. According to predictions of the quasi-steady theory, the forced rotation has been performed for angles of attack ranging from -10 to 20. Rotational amplitudes θ_0 are set between 1 and 20

however for angles of attack equal to $\alpha = -5,0$ those are set ranging from 1 to 25.
Fig.(4.15) shows the fluid flow induced rotational damping as a function of forced rotation amplitude for several values of the angle of attack at rest. As shown in Fig (4.15), the flow fluid damping coefficients are negative for angles of attack at rest of -5 to 5 up to amplitude of around 20 degrees. This observation is similar to forced rotation results from the square section model. We observe that the fluid flow damping coefficients are positive for angles of attack ranging from -5 to -10 and 5 to 15 which have been predicted negative by the quasi-steady criterion. This observation demonstrates once more that the quasi-steady criterion is too conservative.
Added inertia values as a function of forced rotation amplitude are shown in Fig. (4.16). For the bundle section, all the added inertia coefficients are positive over the whole range of the forced rotation amplitudes and angles of attack at rest except for 0 degree angle of attack. Also, as seen in Fig (4.16), the added inertia for the angles of attack -5 and 5 is similar as for the angles of attack -10 and 10.

4.3.3 Direct fluid-structure interaction

In this section, the free rotation around the central axis of bundle is considered. The section is restrained by a torsional stiffness. As discussed in the section on the square prism, equation (4.9) is the governing equation for free rotation. As for the square section, fluid flow and structural rotations are solved fully coupled. The following structure parameters (which are defined per unit length) have been considered :

— $I = I*/(\rho_f D^4) = 4.99$

— $K = 0.123$

The time histories of rotational angles for several values of the angles of attack are shown in Fig.(4.17). From the simulations of free rotation, rotational angles vibrations have been observed at angles of attack at rest ranging from -5 to 15 degrees. These results are not in agreement with the results from the forced rotation, while FSI results are close to the quasi-steady theory. From the time histories of rotation angles, for example when the angle of attack at rest is 10, the observed averaged angle if 5 degrees. A more detailed discussion will be presented in the following summary section.

4.3.4 Summary

The predictions of rotational galloping threshold for square section has been performed based on the quasi-steady criterion, forced rotation and direct FSI simulations see Table (4.2). The quasi-steady theory predicts that rotational galloping occurs at between angles of attack -10 and 15 degrees. The occurrence of torsional galloping based on our three models are identified by Yes

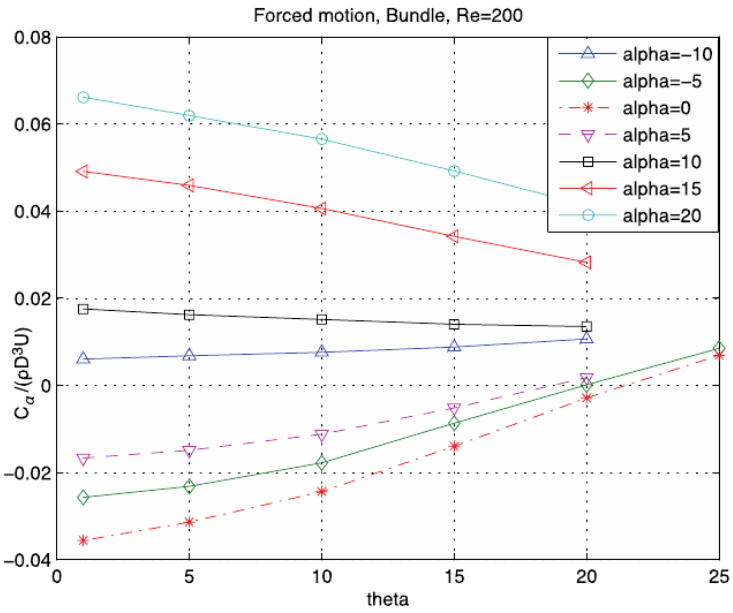

Figure 4.15 Induced fluid flow rotational damping.

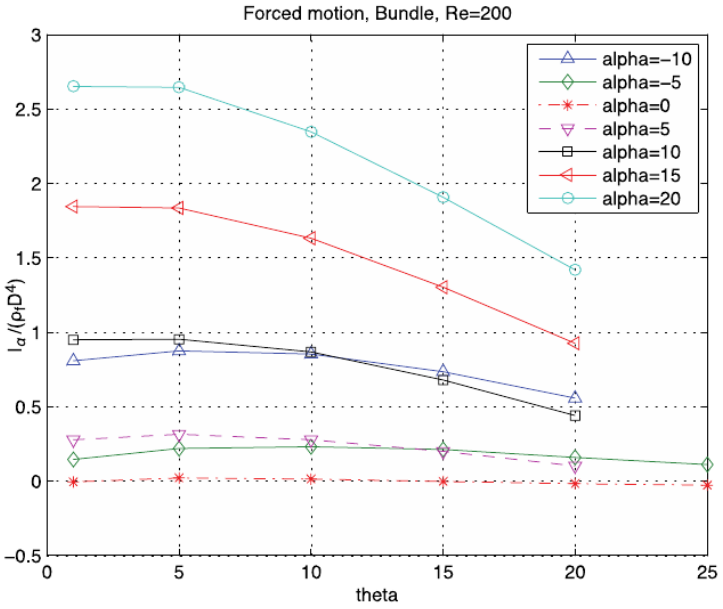

Figure 4.16 Added inertia for the bundle section.

or No in the first 3 columns of Table (4.2). As discussed in previous sections, the occurrence of torsional galloping predicted by quasi-steady criterion and free rotation simulations are in good agreements. For the angles of attack at rest that the threshold of torsional galloping is Yes, the am-

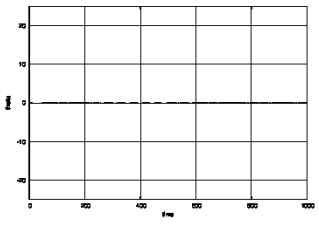

(a) $\alpha = -45$

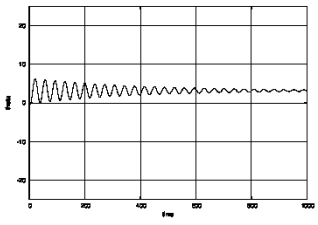

(b) $\alpha = -15$

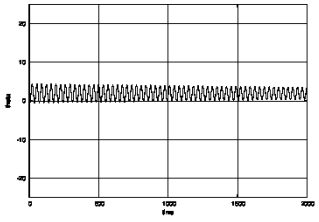

(c) $\alpha = -10$

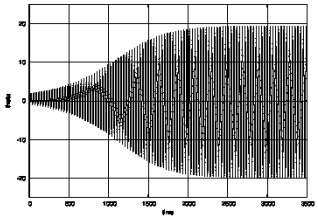

(d) $\alpha = -5$

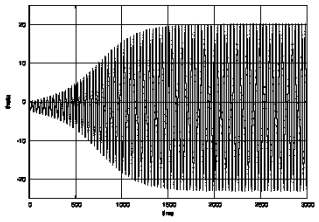

(e) $\alpha = 0$

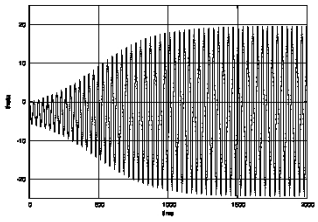

(f) $\alpha = 5$

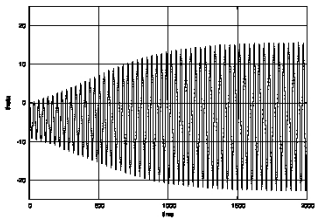

(g) $\alpha = 10$

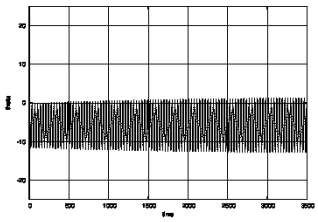

(h) $\alpha = 15$

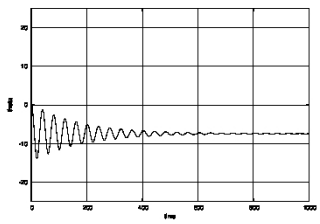

(i) $\alpha = 25$

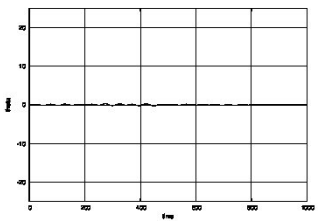

(j) $\alpha = 45$

Figure 4.17 Rotation angle histories of bundle section

plitude of rotations are determined.

The effective angle of attack for several angles of attack are shown in columns 5 and 6. To predict the effective angle of attack of quasi-steady model, the equation (4.10) has been used. Also, to compute the effective angle of attack for the FSI simulations, the equation (4.11) has been used. By comparison between the quasi-steady and free rotation effective angles of attack, we conclude that the quasi-steady and FSI simulations predictions are generally in accordance. Although, we note more pronounced differences between at rest and effective angles of attack for the bundle than for the square section. This can be due to the much lower values for the structural parameters, particularly the torsional stiffness for the bundle. Indeed, the torsional stiffness is 3.35 lower than that of the square section.

The reduced velocity observed in FSI simulations are given in the last column of the Table (4.2). We set the reduced velocity equal to 40. However, the observed reduced velocity is lower for all configurations correspond to the galloping. This can be due to two reasons, first because of the negative flow-induced torsional stiffness. Next, it is due to the quite low added moment of inertia for the effective rotational amplitudes encountered in the FSI simulations in comparison with the solid moment of inertia. Thus, the effects of the flow-induced stiffness is more than the added inertia.

Tableau 4.2 Bundle cylinder rotational galloping threshold based on the models.

AOA α	**QS**	**Forced θ**	**FSI θ_{max}**	**QS α_{eff}**	**FSI α_{eff}**	**FSI U_R**
-25	No	No	No	-21.3	-21.3	
-20	No	No	No	-16.2	-16	
-15	No	No	No	-11.9	-12	
-10	Yes	No	No	-8.1	-8	
-5	Yes	19	19	-4.5	-4	35
0	Yes	22	21	-1.1	-1.4	35
5	Yes	20	20	2.2	2	35
10	Yes	No	17	5.5	5	35.7
15	Yes	No	5	9	9	35
20	No	No	No	13	13	
25	No	No	No	17.7	17.6	

CHAPITRE 5

CONCLUSION

In this work, we have performed simulations of the laminar flow around a square and a bundle section cylinders at $Re = 200$. The threshold of the translational galloping of bundle section cylinder has investigated by considering the quasi-steady criterion and direct fluid structure interaction.
The occurrence of torsional galloping of square and bundle section cylinders has been investigated with three kinds of simulations :

- Fixed body in order to evaluate the quasi-steady criterion,
- forced rotation to determine the induced-fluid flow damping coefficient and added inertia,
- free rotation simulations to determine the response of the structures by solving fully coupled of the fluid flow and structure motion.

All of the simulations were performed by using a finite element method with high spatial and temporal accuracy.

5.1 Discussion

Results from steady simulations of translational galloping of bundle show that no translational galloping occurs for this case. Free transverse motion results validate the quasi-steady prediction. We increased the Reynolds number to 400 but no translational galloping was observed.
Results show that torsional galloping will occur for square and bundle sections over a limited range of angles of attack. The amplitude of rotational galloping reaches a maximum of 25 degrees at $Re = 200$ and a reduced velocity 40. Good agreement has been observed between our results for square section with those of Robertson *et al.* at similar Reynolds numbers.
By comparing predictions from the three models for torsional galloping occurrence, we conclude that the quasi-steady criterion does not predict the same instability range obtained with the other two methods. In fact, we observe an overestimated range of instability. At least the criterion is overly conservative. But, there is no assurance that this criterion preserves this characteristic for other shapes or flow conditions.
Furthermore, there are noticeable discrepancies between forced rotation results and direct FSI. However, by considering the effective angle of attack induced by the averaged moment, comparable instability ranges are observed.

5.2 Future Study suggestions

Galloping phenomenon particularly the torsional galloping is more challenging in simulation and also, its threshold is an important key in designing structures placed in the fluid flow. More work need to be done in order to evaluate the galloping phenomenon and the effective parameters on it. It is believed that the existing finite element method and analysis tools could be extended to :

— simulation of three-dimensional problem

— study the effects of turbulent flow on instability

— study the two-degrees-freedom by considering the translational and torsional galloping

REFERENCES

[1] Jeffery C. Measamer Xi Qu, Tao Qi. Vortex-induced vibration reduction device for fluid immersed cylinders. (US 6948884B2), 09 27, 2005.

[2] M. P. Paidoussis, S. J. Price, and E. de Langre. *Fluid-Structure Interactions Cross-Flow-Induced Instabilities*. Cambridge, New York, US, 2011.

[3] J. P. Den Hartog. *Mechanical Vibrations*. McGraw- Hill, USA, 1956. 299-305 pp.

[4] R. D. Blevins. *Fluid Induced Vibration*. Krieger Publishing Company, Malabar, 2nd edition, 2001.

[5] S. Cheng, G.L. Larose, M.G. Savage, and H. Tanaka. Aerodynamic behaviour of an inclined circular cylinder. *Journal of Wind structures*, 6 :197–208, 2003.

[6] John H.G. Macdonald and G. L. Larose. Two-degree-of-freedom inclined cable galloping part 1 : Analysis and prevention for arbitrary frequency ratio. *Journal of Wind Engineering and Industrial Aerodynamics*, 96 :291–307, 2008.

[7] John H.G. Macdonald and G. L. Larose. Two-degree-of-freedom inclined cable galloping part 2 : Analysis and prevention for arbitrary frequency ratio. *Journal of Wind Engineering and Industrial Aerodynamics*, 96 :308–326, 2008.

[8] G. Alonso, E. Valero, and J. Meseguer. An analysis on the dependence on cross section geometry of galloping stability of two-dimensional bodies having either biconvex or rhomboidal cross sections. *European Journal of Mechanics B/Fluids*, 28 :328–334, 2009.

[9] B. Molin, F. REmy, T. Rippol, A. Cinello, E. le Hir, C. Berhault, and C. Dassibat. Experimental investigation on the galloping response of square cylinders at high Reynolds numbers. In *6th International conference on Hydroelasticity in marine technology*. Tokyo, Japan, 2012.

[10] A. Acampora, J.H.G. Macdonald, C. T.Georgakis, and N. Nikitas. Identification of aeroelastic forces and static drag coefficients of a twin cable bridge stay from full-scale ambient vibration measurements. *Journal of Wind Engineering and Industrial Aerodynamics*, 124 :90–98, 2014.

[11] Y. C. Fung. *An Introduction to the Theory of Aeroelasticity*. Wiley (reprinted by Dover Publications, 1993), New York, USA, 1955.

[12] P. W. Bearman, I. S. Gartshore, D. J. Maull, and G. V. Parkinson. Experiments on flow-induced vibration of a square-section cylinder. *Journal of Fluid and structures*, 1 :19–34, 1987.

[13] B. W. Van Oudheusden. On the quasi-steady analysis of one degree-of-freedom galloping with combined translational and rotational effects. *Journal of nonlinear dynamics*, 8 :435–451, 1995.

[14] J. D. Smith. *An experimental study of the aeroelastic instability of rectangular cylinders*. Phd thesis, University of British Columbia, Vancouver, Canada, 1962.

[15] G. V. Parkinson and J. D. Smith. The square prism as an aeroelastic non-linear oscillator. *Quarterly Journal of Mechanics and Applied Mathematics*, 17 :225–239, 1964.

[16] A. Barrero-Gil, A. Sanz-Andres, and M. Roura. Transverse galloping at low Reynolds numbers. *Journal of Fluids and Structures*, 25 :1236–1242, 2009.

[17] T. Andrianne. *Experimental and Numerical Investigations of the Aeroelastic Stability of Bluff Structures*. Phd thesis, University of Liege UK, 2012.

[18] G.V. Parkinson and N. P. H. Brooks. On the aeroelastic instability of bluff cylinders. *Journal of Applied Mechanics*, 28 :252–258, 1961.

[19] J. E. Slater. *Aeroelastic instability of a structural angle section*. Phd thesis, University of British Columbia, Vancouver, B.C., Canada, 1969.

[20] Y. Nakamura and T. Mizota. Torsional flutter of rectangular prisms. *ASCE Journal of the Engineering Mechanics Division*, 101 :125–142, 1975.

[21] Y. Nakamura and Y. Tomonari. Galloping of rectangular prisms in a smooth and in a turbulent flow. *Journal of Sound and Vibration*, 52 :233–241, 1977.

[22] T. Tamura and Y. Itoh. Unstable aerodynamic phenomena of a rectangular cylinder with critical section. *Journal of Wind Engineering and Industrial Aerodynamics*, 83 :121–133, 1999.

[23] B. W. van Oudheusden. Rotational one-degree-of-freedom galloping in the presence of viscous and frictional damping. *Journal of Fluids and Structures*, 10 :673–689, 1996.

[24] Y. Nakamura and T. Yoshimura. Flutter and vortex excitation of rectangular prisms in pure torsion in smooth and turbulent flows. *Journal of Sound and Vibration*, 84 :305–317, 1982.

[25] M. Studnickova. Vibrations and aerodynamic stability of a prestressed pipeline cable bridge. *Journal of wind engineering and industrial aerodynamics*, 17 :51–70, 1984.

[26] Y. Nakamura and T. Matsukawa. Vortex excitation of rectangular cylinders with a long side normal to the flow. *Journal of fluid mechanics*, 180 :171–191, 1987.

[27] Y. Nakamura. On the aerodynamic mechanism of torsional flutter of bluff structures. *Journal of Sound and Vibration*, 67 :163–177, 1979.

[28] K. Washizu, A. Ohya, Y. Otsuki, and K. Fujii. Aeroelastic instability of rectangular cylinders in a torsional mode due to a transverse wind. *Journal of Sound and Vibration*, 72 :507–521, 1980.

[29] A. S. Richardson, J. R. Martucelli, and W. S. Price. Research study on galloping of electric power transmission lines. part I. In *In Proceedings 1st International Conference on Wind Effects on Buildings and Structures*. Teddington, UK, 1965.

[30] P. Yu, Y. M. Desai, N. Popplewell, and A. H. Shah. Three degrees-of-freedom model for galloping. part I : formulation. *ASCE Journal of Engineering Mechanics*, 119 :2404–2425, 1993.

[31] P. Yu, Y. M. Desai, N. Popplewell, and A. H. Shah. Three degrees-of-freedom model for galloping. part II : solutions. *ASCE Journal of Engineering Mechanics*, 119 :2426–2448, 1993.

[32] P. Yu, N. Popplewell, and A. H. Shah. Instability trends of inertially coupled galloping, part I : initiation. *Journal of Sound and Vibration*, 183 :663–678, 1995.

[33] P. Yu, N. Popplewell, and A. H. Shah. Instability trends of inertially coupled galloping, part II : periodic vibrations. *Journal of Sound and Vibration*, 183 :679–691, 1995.

[34] J. Macdonald and G. Larose. A unified approach to aerodynamic damping and drag/lift instabilities and its application to dry inclined cable galloping. *Journal of Fluids and Structures*, 22 :229–252, 2006.

[35] J. Macdonald and G. Larose. Two-degree-of-freedom galloping. part 1 : General formulation and solution for perfectly tuned system. *Journal of Wind Engineering and Industrial Aerodynamics*, 96 :291–307, 2008.

[36] J. Macdonald and G. Larose. Two-degree-of-freedom galloping. part 2 : Analysis and prevention for arbitrary frequency ratio. *Journal of Wind Engineering and Industrial Aerodynamics*, 96 :308–326, 2008.

[37] R. D. Blevins and W. D. Iwan. The galloping response of a two-degree-of-freedom system. *Journal of Applied Mechanics*, 41 :1113–1118, 1974.

[38] K. Schulz and Y. Kallinderis. Unsteady flow structure interaction for incompressible flows using deformable hybrid grids. *Journal of Computational Physics*, 143 :569–597, 1998.

[39] L. Li, S.J. Sherwin, and P.W. Bearman. A moving frame of reference algorithm for fluid/structure interaction of rotating and translating body. *International Journal for Numerical methods in Fluids*, 1, 2000.

[40] I. Robertson, L. Li, S.J. Sherwin, and P.W. Bearman. A numerical study of rotational and transverse galloping rectangular bodies. *Journal of Fluids and Structures*, 17 :681–699, 2002.

[41] A. P. Singh, A. K. De, V. K. Carpenter, V. Eswaran, and K. Muralidhar. Flow past a transversely oscillating square cylinder in free stream at low reynolds numbers. *International Journal For Numerical Methods In Fluids*, 61 :658–682, 2008.

[42] A. Joly, S. Etienne, and D. Pelletier. Galloping of square cylinders in cross-flow at low Reynolds numbers. *Journal of Fluids and Structures*, 28 :232–243, 2012.

[43] D.H Yoon, K. S. Yang, and Ch. B. Choi. Three-dimensional wake structures and aerodynamic coefficients for flow past an inclined square cylinder. *Journal of Wind Engineering and Industrial Aerodynamics*, 101 :34–42, 2012.

[44] J. N. Reddy. *An Introduction to the finite element method*. McGraw- Hill, USA, 1993.

[45] J. Xin and J. E. Flaherty. Implicit time integration of hyperbolic conservation laws via discontinuous galerkin methods. *International Journal For Numerical Methods In Biomedical Engineering*, 27 :711–721, 2009.

[46] G. Jothiprasad, D. J. Mavriplis, and D. A. Caughey. Higher-order time integration schemes for the unsteady Navier-Stokes equations on unstructured meshes. *Journal of Computational Physics*, 191 :542–566, 2003.

[47] S. Etienne, A. Garon, and D. Pelletier. Perspective on the geometric conservation law and finite element methods for ALE simulations incompressible flow. *Journal of Computational Physics*, 228 :2313–2333, 2009.

[48] L. Charlot, S. Etienne, and D. Pelletier. Verification of a free surface adaptive finite element solution algorithm. In *49th AIAA Aerospace Sciences Meeting Including The New Horizons Forum And Aerospace Exposition*. Orlando, Florida, 2011.

[49] Zh. Yang and D. J. Mavriplis. Higher-order time integration schemes for aeroelastic applications on unstructured meshes. *AIAA Journal*, 45 :138–150, 2007.

[50] A. Malidi, A Dufour, and D. N'dri. A study of time integration schemes for the numerical modelling of free surface fows. *International Journal for Numerical Methods in Fluids*, 48 : 1123–1147, 2005.

[51] G. Damblans, C. Berhault, C. Le Cunff, B. Molin, P. Wiet, A. Cinello, T. Deglaire, and J-L. Legras. In *Investigations on galloping of non-circular cross-sections*, volume 7. Nantes, France, 2013.

[52] O. Schenk and K. Gärtner. Solving unsymmetric sparse systems of linear equations with pardiso. *Journal of Future Generation Computer Systems*, 20 :475–487–1147, 2004.

[53] O. Schenk and K. Gärtner. On fast factorization pivoting methods for symmetric indefinite systems. *Electronic Transactions on Numerical Analysis*, 23 :158–179, 2006.

[54] A. R. Bokaian and F. Geoola. Hydroelastic instabilities of square cylinders. *Journal of sound and vibration*, 92 :117–141, 1984.